

Characteristics of Metamorphic Textures of the Loch Eil Group of the Moine Highlands

ERTH 4104 & ENVS 4901 Earth and Environmental Science Undergraduate Research Proposal

Prepared by: Julie Woods

Supervisor: Dr. Richard Cox
Dalhousie University, Halifax, NS
Course Coordinator: Dr. Tarah Wright
Associate Professor of Environmental Science
Dalhousie University, Halifax, NS

Acknowledgements

I would like to thank Dr. Richard Cox for his continuous support and guidance throughout the duration of the research project, as well as Dan MacDonald for his help with the major element analysis of our samples. I would like to recognize the students of EARTH 2001 with their assistance in the data collection, and finally, I would like to thank Dr. Tarah Wright for her guidance throughout the semester and aiding with writing affective research proposals.

Table of Contents

1. Abstract.....	iv
2. Introduction.....	1
2.1 Background.....	1
2.2 Context.....	3
3. Literature Review.....	4
3.1 Geochronology.....	4
3.2 Tectonostratigraphy.....	5
3.3 Stratigraphy.....	7
3.4 Metamorphic History.....	8
4. Methods.....	11
4.1 Methodology.....	11
4.2 Limitations.....	15
5. Results.....	16
5.1 Sample Description.....	16
5.2 X-Ray Mapping.....	18
5.2 Metamorphic Constraints.....	19
5.2.1 Mineral Classifications.....	19
5.2.2 Garnet-Chlorite Geothermometry.....	28
5.2.3 Garnet-only Geobarometry.....	29
5.2.4 Garnet-Biotite-Plagioclase-Quartz Geobarometer.....	30
6. Discussion.....	33
7. Supplementary Data.....	37
8. References.....	38

1.0 Abstract

Recent studies on the Moine supergroup suggests that ages over a large extent have been poorly constrained, and lack of research conducted is a result of structural complexity and mineralogical monotony. The purpose of this research is to fill in said gaps in knowledge and data, with the following research question: how many metamorphic events are being recorded in the rocks of the southern Moine highlands. It is hypothesized that there are 2 events at 800 Ma, caused by different phases of the Knoydart event, 1 event at 450 Ma, caused by the Caledonia event, and possible contact metamorphism at 425 Ma, caused by the Strontian granitic intrusions. The methodology being implemented consists of microscope analysis to broadly identify mineral assemblages and metamorphic textures in the samples, followed by major element analysis on the microprobe, which is then proceeded by x-ray mapping of garnet grains present in the samples, U-Th-Pb analysis of monazite grains to help establish a range of ages, and geothermobarometric modelling to establish temperature and pressure conditions of the samples. For the purpose of this analysis, garnet geothermobarometers such as GASP, GMBP, and garnet-biotite-plagioclase-quartz will be used, and the data being inputted into the models will be extract from major element analysis. The mineral assemblages present in the four samples being used in the analysis show varying percentages of quartz, feldspars, and micas, with garnet and monazite being abundant in one sample. Primary metamorphic textures present in the samples are symplectite, undulatory extinction, and schistosity. Current limitations are due to overprinting, which affects age precision, distinguishing between older and younger fabrics, and deciphering between competing P-T-t paths, as well as lack of aluminosilicates in the samples as another limitation. Through geothermobarometric modelling, it has been determined that the temperatures being recorded are ranging from 550-660°C with some outliers plotting around 750°C, and the pressure conditions are ranging from 2-8 kbar, with most of those pressure conditions ranging from 3-5 kbar.

Keywords: Moine, garnet, monazite, geothermometry, geobarometry

2.0 Introduction

The motivation to complete this research was to close any gaps in knowledge regarding the metamorphic events that interacted with the Loch Eil group, and to determine the number of metamorphic events that deformed the rocks of the southern Moine highlands; the primary area of focus is located in Glen Tarbert, about 6 km west of Loch Linnhe. This research is important as it has been noted that ages over a large tract of the Moine highlands have been poorly constrained, as well as the lack of research that has been conducted is due to the mineralogical monotony and its structural complexity (Cawood et al., 2014; Soper et al., 1998). Here we will examine the mineral assemblages, the dominant and secondary fabrics, and the P-T conditions being recorded in the samples of the Loch Eil and Glenfinnan group of the Moine highlands.

Background

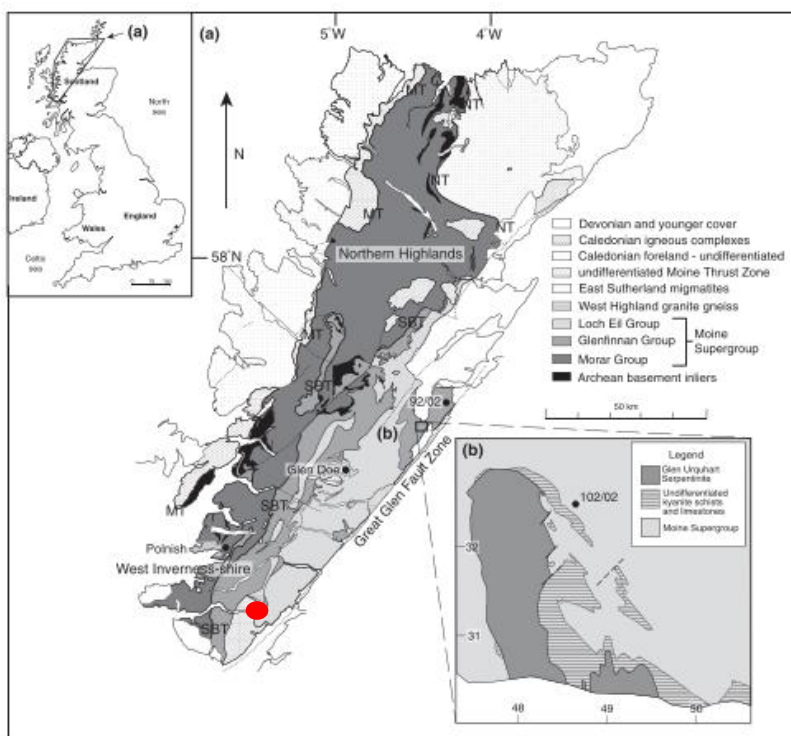


Figure 1. Area in which the Moine Supergroup is located. The circle denotes where the study area is located for the Loch Eil analysis. Source: K.A Cutts, et al., 2010

The Moine Supergroup is a sequence of Neoproterozoic aged meta-sedimentary rock located in the Northern Highlands Terrane between the Moine Thrust and Great Glen Fault and is comprised of three main lithostratigraphical units: from oldest to youngest, the Morar, the Glenfinnan, and the Loch Eil groups (Cutts et al., 2010). The focus of this research is on the Loch Eil group with some emphasis on the Glenfinnan; the

stratigraphy of the Moine suggests that the Loch Eil superimposes the Glenfinnan group, with

it the top of the Loch Eil section cannot be seen. Overall, the Moine Supergroup is over 10 kilometers in thickness (Cawood et al., 2004). The Moine Supergroup is composed primarily of Neoproterozoic meta-sedimentary rocks such as metapelites, which have a clay-rich protolith, generally shales or mudstones, as well as psammites and quartzites. Psammites and quartzites both have the same protolith—sandstones—however the primary difference between the two is that psammites have feldspars and micas along with quartz as part of their mineral assemblage, whereas quartzites are over 90% quartz. Through decades of research from various authors, such as C.L Kirkland (2008) determined that the Moine rocks were deposited between 1 Ga and 870 Ma, which was also around the time when the oldest meta-igneous intrusions were emplaced in the Supergroup; these rocks likely were deposited around the northeastern margin of Laurentia and then eroded during the Grenville Orogeny, which occurred in 1.1-1.0 Ga when Rodinia, the supercontinent, was forming (Cutts et al., 2010). This age range was determined through the lack of fossiliferous material present in its stratigraphy, which is consistent with a Precambrian deposition, as well as the complete lack of deformation from the Grenville orogeny, which occurred at 1.3-1.0 Ga; this information was used in conjunction with detrital zircon ages (Cutts et al., 2010). The Knoydartian event has been dated as 820 Ma to 740 Ma during the Neoproterozoic and has been determined to be poorly constrained, and its origin has yet to be established (Krabbendam et al., 2014). The Caledonian orogeny, which occurred at 470-430 Ma, resulted in the closing of the Iapetus Ocean when the Baltican, Laurentian, and Avalonian terranes collided. This tectonic event was determined to have two phases: the first phase occurring in the early Ordovician which resulted in the Grampian event with continental collision. The second phase, which occurred in the Silurian, resulted in the colliding of Laurentia with another paleocontinent called Baltica. This was denoted as the Scandian event (Cutts et al., 2010). The Caledonian orogeny also emplaced the Strontian Granites around 425 Ma, which have further deformed the rock samples produced in the area (Hutton, 1988).

In a paper by K.A Cutts (2010), it was stated that pressure-temperature constraints, as well as monazite ages were determined through geochronological modelling; metamorphic constraints that were determined through models such as a garnet-biotite-plagioclase-

chlorite-staurolite-quartz-ilmenite-H₂O geothermobarometric model has ascertained pressures ranging from about 6 kbar to approximately 7 kbar, with the pressure increasing to 8-9 kbar in different garnet zones. Temperatures have been determined to be ranging from 600-650°C in the lower pressure, with it increasing to approximately 700°C in the higher-pressure readings. In terms of the ages that were constrained using in situ LA-ICPMS analysis of the monazite grains in the samples, two types of monazite grains are investigated: matrix monazites (monazites growing in the matrix) and monazite that grew as inclusion in the garnet grains. ²⁰⁶Pb/²³⁸U readings from the monazite inclusions in the garnets yielded ages ranging from 464 ± 1.5 to 825 ± 18 Ma, depending on which zone and garnet the grain has grown in. In terms of the matrix monazites, ²⁰⁶Pb/²³⁸U readings are approximately 462 ± 2 Ma; the validity of these ages is verified through U-Pb zircon geochronology, which yields ²⁰⁷Pb/²⁰⁶Pb readings of approximately 724 ± 6 Ma (Cutts et al., 2010).

2.2 Context

The goal of this research is to differentiate the metamorphic events that had taken place in the area and observe the overprinting of the dominant and secondary fabrics as a result of these orogenies, which will aim to answer the primary question: how many metamorphic events are being recorded in the samples from Glen Tarbert, as well as what do the metamorphic textures present in the samples tell us about the metamorphic event. It is hypothesized that there are 2 events at 800 Ma, which was the Knoydartian event, and its different phases, 1 event at 450 Ma, which was the Caledonian event, and possible contact metamorphism from the Strontian granitic complex at 425 Ma.

The scope of this study is centered in the northwestern area of the Northern highland terrane, 11 km west of the Great Glen Fault, and 40 km southeast of the Moine Thrust. Our research will be primarily focused on Glen Tarbert, one of the few places in Scotland where both orogenies can be observed in the primary and secondary metamorphic fabrics. As mentioned previously, the time period at which these two orogenies took place ranges from the Neoproterozoic to the mid to late Cambrian period, and a detailed analysis will be conducted over a period of a year. The research question will be addressed with the following

methodology: firstly, by broadly identifying mineral assemblages and metamorphic textures present in each of the 4 thin sections using microscope analysis. This will be followed with in-depth major element analysis of the mineral assemblages in each sample, which will then be inputted into our geothermobarometric models; this will be conducted with the use of the electron microprobe. The geothermobarometry will be used to help constrain P-T conditions of the samples. Following this, a selection of garnet grains present in the samples will undergo detailed mapping of the Ca, Fe, Mg, Y, and Mn concentrations, which will also aid in constraining P-T conditions.

3.0 Literature Review

3.1 Geochronology

When it comes to interpreting the chronology and the process of chemical reactions in medium to high-grade metamorphic rocks, garnets are one of the most useful minerals to analyze, however, without a proxy it is restricted in its use. In a paper by K.T Ashley (2017), it states that thermobarometric calculations are facilitated by the chemical exchange and equilibrium between garnet and other minerals present in a given mineral assemblage. Relative timing between the growth and deformation of a garnet can be inferred by the inclusion trails in the grain. As well, pressure shadows give shear sense direction and any minerals found in the garnet grains can provide evidence of burial and exhumation histories of the rock package as a whole. Due to the multiple growth phases, producing either small grains, zoning or overgrowths, garnets are restricted in its geochronological uses, as well as laboratory preparation and measuring its isotopic data is expensive and time consuming. Because of this, it limits the number of samples that can be processed (Ashley, K. T, et al., 2017). Garnets are paramount in yielding in-depth pressure-temperature conditions in metamorphic environments, which can help to provide information on the tectonic evolution of geological terranes, however they are limited there use without a proxy.

The metasedimentary rocks from the Moine supergroup, located in the frontal ductile thrust sheets of the wedge produced during the Caledonian orogenic event are currently extremely limited in the geochronological data that is being measured from the garnets and

other indicator minerals found within its mineral assemblage. There are instances where few of the garnet analyses have yielded ages that do not coincide with previous age groups that have been produced from the isotopic measurements from other metamorphic minerals that have been analyzed and grouped to major orogenic events. This is especially so when examining other metamorphic petrology studies that concern garnet chemistry being used to understand the P-T histories and thermal evolution of the Scandian (phase of the Caledonian orogenic event) metamorphic events with the aid of garnet analysis from the major orogenic events that predate (Knoydart and Grampian) its event. Unless the Scandian heating was high enough to re-equilibrate the garnet's chemical information to reflect Scandian P-T conditions. Because of these inconsistencies with the isotopic data, quantifying P-T histories from these orogenic events becomes very difficult (Ashley, K. T, et al., 2017; Bird, A. F et al., 2013). The frontal ductile thrust sheet of the Moine supergroup produced during the Caledonia orogenic event is limited in the geochronological data being produced from the garnets and indicator minerals present in its mineral assemblage and poses a problem when quantifying its P-T histories, producing inconsistencies in isotopic data.

3.2 Tectonostratigraphy

Identifying the tectonic setting in which crustal thickening and extension during metamorphic processes are occurring is paramount in investigating tectonic events, as well it is important in understand the mechanisms that drive differentiation in continental crust. In a paper titled "Extensional versus compressional setting for metamorphism: Garnet chronometry and pressure-temperature-time histories in the Moine Supergroup, northwest Scotland" written by D. Vance in 1998, they concluded that extension and crustal thickening are two contrasting tectonic events that results from the disturbances in continental geotherm, producing large-scale regional metamorphism. Distinguishing which two are at play is not simple as structural constraints are ambiguous. Problems that arise in polyorogenic terranes are partial or complete overprinting of metamorphic fabrics and structures that were produced in earlier events by those formed in later events. When this occurs, using both structural observations and isotopic studies in relation to P-T paths in conjunction with directly dating the mineral paragenesis, is very useful in resolving any ambiguity in tectonic setting of

major tectonothermal events (Vance D., 1998). In another paper written by M. Sandiford and R. Powell titled “Deep crustal metamorphism during continental extension”, they state that it has been determined in recent studies that metamorphic fabrics and structures from basement terranes form during extension, contrary to what was previously assumed: crustal thickening (Sandiford, M and Powell, R, 1986). It is important to identify the tectonic settings that have crustal thickening and extension during metamorphic processes, because they can aid in investigating tectonic events, as well as understanding the mechanisms behind crustal differentiation in continental crust. Problems that may occur in polyorogenic terranes, like the Moine, are partial and complete overprinting of earlier events by later events but can be resolved by using isotopic studies and P-T paths.

The Moine supergroup has had little research conducted on its tectonostratigraphy due to its structural complexity, as well as its monotonous lithology. In a paper written by N.J Soper in 1998, they conclude that regional stratigraphy for the Moine supergroup has been conducted in recent years, as well as studies on sedimentology in areas where low-strain rates have been recorded, and these studies have shed light on the depositional environment in which the two thickest sandstone sequences in the Moine were deposited. These sequences are the Loch Eil psammite, and the Upper Morar psammite (Soper, N. J, Harris, A. L, Strachan, R. A, 1998). Despite the fact that the tectonostratigraphy of the Moine supergroup has had little analysis conducted due to its structural complexity and monotonous lithology, the studies that are being conducted are helping to shed some light on the conditions at which some of the sequences have been deposited.

3.3 Stratigraphy

The metasedimentary rocks that comprise the Moine supergroup, located in the Northern highland Terrane in northern Scotland, are bounded to the Moine Thrust Zone, situated to the northwest, and to the Great Glen Fault, which is situated to the southeast. There are three stratigraphic units that comprise the Moine supergroup, and they are as followed, from east to west and in ascending order: the oldest being the Morar group, the Glenfinnan group, and the youngest being the Loch Eil group. The sediments that compose

each of the groups were deposited and accumulated on the Laurentian margin, which was a result from the early Neoproterozoic extension of the lithosphere in the post-Grenvillian basins. Various scientific papers have concluded that isotopic age dating from detrital and inherited zircons found in the Moine thrust sheet (Morar group) produced ages ranging from 1650-1100 Ma, thus suggesting a late Proterozoic and Grenville-age provenance (Ashley, K. T, et al., 2017; Friend, C.R.L, et al., 1997, 2003; Cawood, P. A, et al, 2015). The Moine supergroup, located in the Northern Highland Terrane in northern Scotland, is comprised of metasediments which have a provenance of late Proterozoic and Grenville-age. These metasediments are bounded to the Moine Thrust Zone, northwest of the Moine supergroup and to the Great Glen Fault, which is situated to the southeast.

The Moine supergroup is comprised of strongly deformed and metamorphosed sedimentary units, composed of psammites and pelites, and are divided into the following units from oldest to youngest: Morar, Glenfinnan, and Loch Eil groups. Various authors have concluded that the sediments that comprise the Moine supergroup are theorized to have been deposited in half-graben sequences trending NNE and were bounded to the west by east-dipping normal faults. The Morar group—the oldest—is composed of a 5km thick psammite and appears to be thickening to the west, as well as complex sand waves, bi-directional crossbedding and gravel lag deposits from both fluvial and shallow marine setting are also present in its composition. The Upper Morar group fine eastwards into the Glenfinnan group, which is comprised of pelitic rocks. Finally, the Loch Eil group is a 4-5km thick sequence composed of psammites and quartzites, and presents with asymmetrical facies distribution, as well the westward thickening could be indicative of renewed lithospheric extension. The Loch Eil group was likely deposited in a shallow marine environment, which is backed up by the presence of bi-directional crossbedding, lenticular and flaser bedding, and wave ripples (Cawood, P.A, et al., 2004; Strachan, R.A, 1986; Glendinning, N.R.W, 1988; Soper, N.J, et al. 1998). The sedimentary rocks of the Moine supergroup are strongly deformed and metamorphosed, composed primarily of psammites and pelites. They are divided into the following units: the Morar, Glenfinnan, and Loch Eil groups.

3.4 Metamorphic History

Metamorphism and deformation of the Moine supergroup occurred during the Knoydart Orogeny, and the subsequent overprinting occurred during the Caledonian orogeny, which is associated with the closure of the early Proterozoic Iapetus Ocean (mid-Ordovician Grampian phase in 470 Ma). The major ductile thrust sheet within the metasedimentary rocks of the Moine supergroup developed when the mid-Silurian collision (430 Ma) of Baltica into the Laurentian margin (Scandian phase); this collision culminated into the development of the Moine Thrust Zone and marked the western margin of the Caledonia orogenic wedge. The Caledonia orogenic wedge is comprised of mylonitic quartzo-feldspathic gneiss (protolith is Lewisian in age), sandstones from the Neoproterozoic, and Cambro-Ordovician shales and limestones. Three major ductile thrust sheets overlay the anchizonal (anchizone: transition between diagenesis and metamorphism), which are the Moine, Naver, and Skinsdale in ascending order; they are located in northern Scotland, and may be imbricated with other, smaller thrust sheets. The Sgurr Beag thrust sheet, which is located to the south of Scotland, may be structurally the same to the Naver and Skinsdale thrust sheets (Ashley, K.T, et al., 2017). The sedimentary sequences of the Moine supergroup were metamorphosed and deformed during the Knoydartian Orogenic event and overprinting of the metamorphic fabrics occurred during the closure of the early-Proterozoic Iapetus Ocean, which was known as the Caledonian orogenic event (mid-Ordovician Grampian phase in 470 Ma).

The tectonic history of a terrane can be effectively estimated with the aid of pressure-temperature (P-T) readings in conjunction with geochronological measurements, especially when considering terranes that have experienced numerous metamorphic events that have completely altered the mineral assemblages, along with their growth histories. Various authors have concluded that P-T conditions of polymetamorphic histories are largely reliant on modeling the evolution of the rock package, as well through calculated phase diagrams. This can be done in lieu or in conjunction of using mineral assemblages for direct P-T calculations. This is called inverse modelling. Even once the P-T conditions are estimated, the tectonic interpretation of the metamorphic sequences can still be ambiguous; with this in mind, tectonic settings can be pin-pointed using paleo-geothermal gradients suggested by P-T conditions

(Cutts, K. A, et al., 2009; Spear, 1993; Brown, 2006, 2007). P-T conditions in conjunction with geochronological measurements can be instrumental in estimating the tectonic history of a geological terrane, especially when that terrane has undergone numerous metamorphic events and the mineral assemblages have been obliterated, along with their growth histories.

The Caledonian orogenic event, which occurred at 470-430 Ma, has been accepted due to the isotopic ages from the regional metamorphism, as well as the mineral assemblages that have been synthesized from the deformed meta-igneous intrusions. K.A Cutts (2010) concluded that the Caledonian event, which closed the Iapetus Ocean in the early-Proterozoic, has been subdivided into two phases: the Grampian event which had occurred during the early to mid-Ordovician as an arc-continent collision, it was then followed the collision of eastern Laurentia with Baltica, which happened in the Silurian and is named the Scandian event (Cutts K.A, et al., 2010). Isotopic ages from the regional metamorphism and their associated mineral assemblages from deformed meta-igneous intrusions have long been the basis for the Caledonian orogenic event, which occurred at 470-430 Ma. This orogenic event has been subdivided into two phases, the Grampian and the Scandian event.

The Glenfinnan and Loch Eil groups of the Moine supergroup were intruded by the igneous protoliths of the West Highland Granitic Gneiss (Fig. 1), and other metabasic rocks at 870 Ma (late Proterozoic). Geochronological data shows that the Moine supergroup, as well as another group east of the Great Glen Fault (Badenoch group), the West Highland Granitic Gneiss and the associated mafic rocks, were affected by Neoproterozoic tectonothermal events, which spanned from 840-725 Ma. These events were known as the Knoydartian event, which was likely split into different phases rather than one great event lasting 100 million years (Cawood, P.A, et al., 2010, 2014; Bowes, D.R, 1968). The West Highland Granitic Gneiss and other metabasic rocks intruded the Glenfinnan and Loch Eil of the Moine supergroup at 870 Ma, which was the late Proterozoic.

The study of the Moine area was deemed important due to the multiple deformation events, this all before isotopic studies into the area revealed the previously unrealized complexity in its orogenic and structural history. In a paper by P.A Cawood (2014) states that

the D₁–D₂ events have been used in the context of separating the different deformational sequences which have occurred in many parts of the Moine supergroup and have been mapped in detail. These D₁–D₂ events each may be associated different sets of tectonic structures. Assigning tectonic structures to certain orogenic events has been made easier using isotopic dating of igneous intrusions, however due to some of the data that has been synthesized from a number of metamorphic porphyroblasts and other accessory phases to the tectonic fabrics, some of the ages have remained ambiguous. This has brought forth the conclusion that many of the ages obtained from isotopic data pulled from tectonic structure and mineral assemblages are poorly constrained over a large portion of the Moine (Cawood P.A, et al., 2014). Due to the polymetamorphic history of the Moine supergroup, it was deemed crucial to study its terrane, however the previous unrealized complexity in its orogenic and structural history have poorly constrained the ages pulled from isotopic data over a large tract of the Moine.

4.0 Methods



Figure 2. Image from Google Earth, showing where the samples (blue dots) are located in conjunction to the study area (yellow star): Glen Tarbert. Source: Map created by Julie Woods

4.1 Methodology

The process by which the samples were analyzed began with in-depth microscope analysis to broadly identify what mineral assemblages and metamorphic textures are present in each thin section. Identification of prominent minerals assemblages and associated metamorphic textures aided in ascertaining approximate pressure and temperature conditions under which the samples were formed, as well as give indication of metamorphic processes, i.e., contact vs. regional metamorphism; this is important as this paper aims to distinguish all tectonic events that have acted on these samples, which included both contact and regional metamorphism.

The following step was to perform major element analysis of the mineral assemblages in the samples on the electron microprobe, which was then be inputted into thermobarometric formulas for calculating pressure-temperature conditions of the tectonic events that have deformed the samples. This will be done using a pre-determined set of formulas that were compiled on an excel spreadsheet, called “P-T Quick”, and is organized based on whether the formula is for pressure, temperature, or for oxides. The validity of this method is sound due to the fact that every formula that is present in this spreadsheet references the peer-reviewed, scientific paper that the information of the model and the formula itself was pulled from; these processes are called geothermometric and geobarometric modelling, which explains the process of estimating pressure and temperature conditions at formation equilibrium. Geothermometry estimates the change in temperature at a constant pressure, and geobarometry estimates the change in pressure over a constant temperature.

For the purpose of this analysis, a garnet-chlorite geothermometer was used to estimate changes in temperature at constant pressure during deformation of the sample. This model utilizes the concentrations of Mg and Fe in the garnet and chlorite grains, which are then used to calculate the partition coefficient and then inputted into the final formula for temperature:

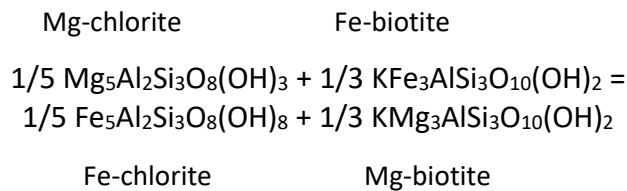
$$\frac{2190.92 + 0.0068 (P \times 1000)}{[0.6867 - \ln(k)] - 273}$$

As well for this calculation, pressure values calculated from the two geobarometers were used. This formula was initially applied in the paper titled “Chloritoid-bearing rocks associated

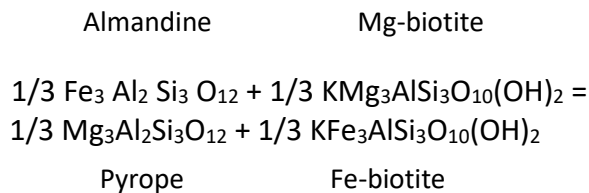
with blueschists and eclogites, northern New Caledonia” written by E. Ghent in 1987. See Ghent’s paper for supplementary formulas for calculating the partition coefficient; this geothermometer is only being used for sample Z2 as it is the only sample with significant amounts of chlorite. This method of calculating temperatures for Z2, Ghent et al. states that chlorite and biotite fractionate both Fe and Mg in a relatively small, and constant rate. Calibration of the exchange equilibrium would make it possible to combine it to obtain the Fe-Mg exchange equilibrium for garnet-chlorite from the Fe-Mg garnet-biotite and get a geothermometric calculation. Calibrating this geothermometer requires Mg-Fe analysis for both garnet and chlorite; these values will be used to calculate the equilibrium constant (K) with the following formula:

$$\frac{Mg(grt)/Fe(grt)}{Mg(chl)/Fe(chl)}$$

The equilibrium constant, as well as pressures for the sample are then inputted into the above equation. The reaction that explains the exchange follows:



and for the equilibrium,

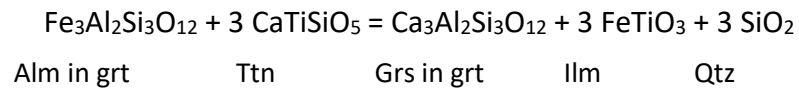


For calculating pressure conditions for the samples, two geobarometers were applied: a garnet-only, and a garnet-biotite-plagioclase-quartz geobarometer. The garnet-only barometer utilized the Ca, Fe, Mg, Mn concentrations in the garnet grains from Z2 and 14, as

well as a list of estimated temperature values from previous analysis to calculate pressure conditions. The following formula was the final calculation applied to estimate a set of pressure conditions:

$$\frac{-8904.5 + 24.542 (T + 273.15) + 0.45R(T + 273.15) \ln \left(\frac{X_{grtCa}}{X_{grtFe}} \right) + 0.15a(T + 273.15) + 0.15c}{1 - 0.15b}$$

This formula was first used in a paper titled “Original Calibration of a Garnet Geobarometer in Metapelite” written by C.M Wu in 2019. See appendix of Wu’s paper for supplementary formulas for the other coefficients. This method for calculating pressures for Z2 and Z14, Wu et al. states that the exchange equilibrium for this geobarometer follows:



where quartz is assumed to be in a pure phase, and both oxides are very near to being in a pure phase, so can be omitted from the calculation; when combined with the thermodynamic equilibria will give the above equation. The calibration required for this model involves calculating the molar fractions for Ca, Fe, Mg, and Mn in the garnet grains. These values are then used to calculate the other coefficients to be inputted into the above formula for pressure.

The Garnet-Biotite-Plagioclase-Quartz geobarometer is utilized by estimating the changes in pressure during the equilibrium exchange between Mg and Fe-rich end-members for garnet and biotite, with the inclusion of plagioclase and quartz. This geobarometer assumes that quartz has formed in a pure phase, therefore the calculation can proceed without needing quartz values; this model has been calibrated under the assumption that the temperature conditions range from 515-878°C, and pressure conditions range from 1.0-11.4 kbar (Wu et al., 2004). Upon major element analysis of the garnet, biotite, and plagioclase grains in the samples, the respective weight percentages for each mineral (garnet: Ca, Mg, Fe, Mn; biotite: Al, Mg, Fe, Ti; plagioclase: Ca, Na, K) are then inputted into various equations to calculate equilibrium constants, and molar fractions, and then finally, the pressure conditions for the samples are calculated with the following two formulas:

P (1)

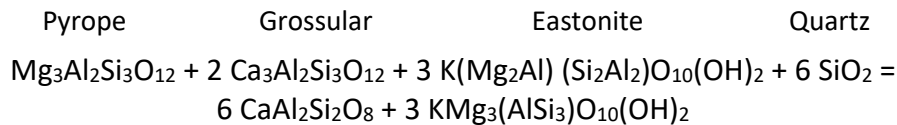
$$\frac{-24450.7 + 40.238 (T + 273.15) + 59256.2 (X_{bioFe}) + 5173.9 (X_{bioMg} - X_{bioAl}) + 6393.4 (X_{bioTi}) + 0.081 [(T + 273.15) (-R \ln K1 - 6Fa + Mga + 2Caa - 788.7(X_{bioFe}) - 6Fc + Mgc + 2Cac)]}{[1 - 0.081 (-6Fb + Mgb + 2Cab)]}$$

P (2)

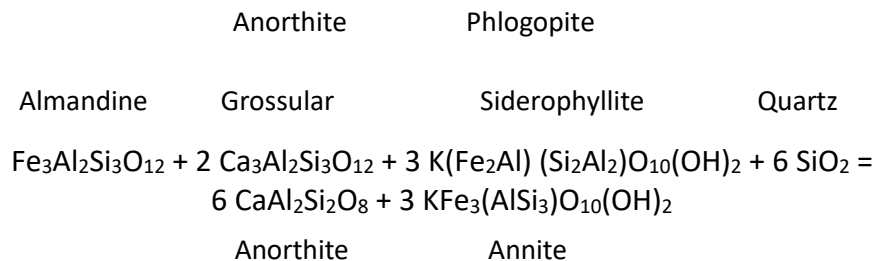
$$\frac{-19871.0 + 30.75 (T + 273.15) + 66622.5 (X_{bioFe} - X_{bioAl}) + 1363.1 (X_{bioMg}) - 74704.2 (X_{bioTi}) + 0.081 [(T + 273.15) (-R \ln K2 - 6Fa + Fea + 2Caa - 840.9 (X_{bioFe}) + 52.2 (X_{bioMg}) + 840.9 (X_{bioAl}) + 1111.2 (X_{bioTi})) - 6Fc + Fec + 2Cac]}{[1 - 0.081 (-6Fb + Feb + 2Cab)]}$$

See C.M Wu's paper titled "Empirical Garnet–Biotite–Plagioclase–Quartz (GBPQ)

Geobarometry in Medium- to High-Grade Metapelites" for the supplementary formulas for calculating the molar fractions and equilibrium constants for this geobarometer. This model utilized the pressure and temperature conditions of both the core and the rim of each of the garnet grains that were analyzed in Z14. The reaction for this geobarometer proceeds with the following Mg and Fe exchange reaction:



and,



X-ray mapping of a selection of garnet grains was also conducted on samples Z2 and Z14, which was produced from the electron microprobe during the major element analysis. The method of this analysis consists of mapping of the Ca, Fe, Mg, Y, and Mn concentrations in garnets from core to rim, as well as the surrounding biotite and plagioclase grains. This helps with understanding the pressure and temperature conditions under which the garnet and the surrounding grains were formed at time of deformation.

4.2 Limitations

The limitations that are present in the overall analysis of this research are primarily due to the overprinting as a result of the polyorogenic terrane that is the Moine supergroup. This entails difficulty in ascertaining different metamorphic fabrics that are associated with each tectonic event and distinguishing between each of them, as well the overprinting makes deciphering between competing pressure-temperature paths of certain minerals assemblages difficult. Any future analysis that may be conducted to determine age of the samples will also be difficult, and with likely only present the most recent metamorphic event in the age dating analysis. Another limitation is due to the lack of aluminosilicates present in the mineral assemblages in the samples. Aluminosilicates such as andalusite, kyanite, and staurolite possess very specific pressure-temperature conditions that need to be met and sustained in order for them to form. Since there is a lack of these indicator minerals, it is very hard to decipher the P-T conditions of the samples without other types of analysis.

5. Results

5.1 Sample Descriptions

1. The Z2 sample represents a psammite from the Loch Eil group, which is a metamorphosed sandstone, composed of quartz, potassium-feldspar, plagioclase feldspar, and chlorite as its primary mineral assemblage, and also includes some oxides, small garnet, and zircon grains. The metamorphic textures present in the sample consists of schistosity of the chlorite, undulatory extinction of the quartz grains. There are also small amounts of symplectite.
2. The Z11 sample represents a metapelite, which is a metamorphosed shale/siltstone/mudstone, composed of mostly quartz, potassium and plagioclase feldspar, and chlorite as its primary mineral assemblage, and includes other minerals such as oxides, small amounts of biotite and muscovite (replacing the chlorite), monazite, and apatite. The metamorphic textures present in this sample are schistosity in the chlorite and biotite, symplectite, and undulatory extinction of the large quartz grains, much like Z2.

3. The Z13 sample represents a quartzite, which is a metamorphosed sandstone, composed of >90% quartz, with minimal amounts of biotite, plagioclase, and potassium feldspar, as well as some very small amounts of muscovite that is replacing the biotite grains. The metamorphic textures present in the sample are undulatory extinction, and schistosity of the biotite, but no symplectite.
4. The Z14 sample represents a biotite-garnet schist from the Glenfinnan group, which is a metamorphosed clay-rich sedimentary rock, composed of garnet, biotite, potassium and plagioclase feldspars, and quartz as the primary mineral assemblage, as well as many small monazite grains. The metamorphic textures present are large amounts of symplectite, schistosity and crenulations of the biotite grains and breaking down of the garnet grains. The quartz grains present in this sample shows uniform extinction, unlike the other 3 samples. The following figures are of the Z2 and Z14 samples, highlighting minerals assemblages and textures:

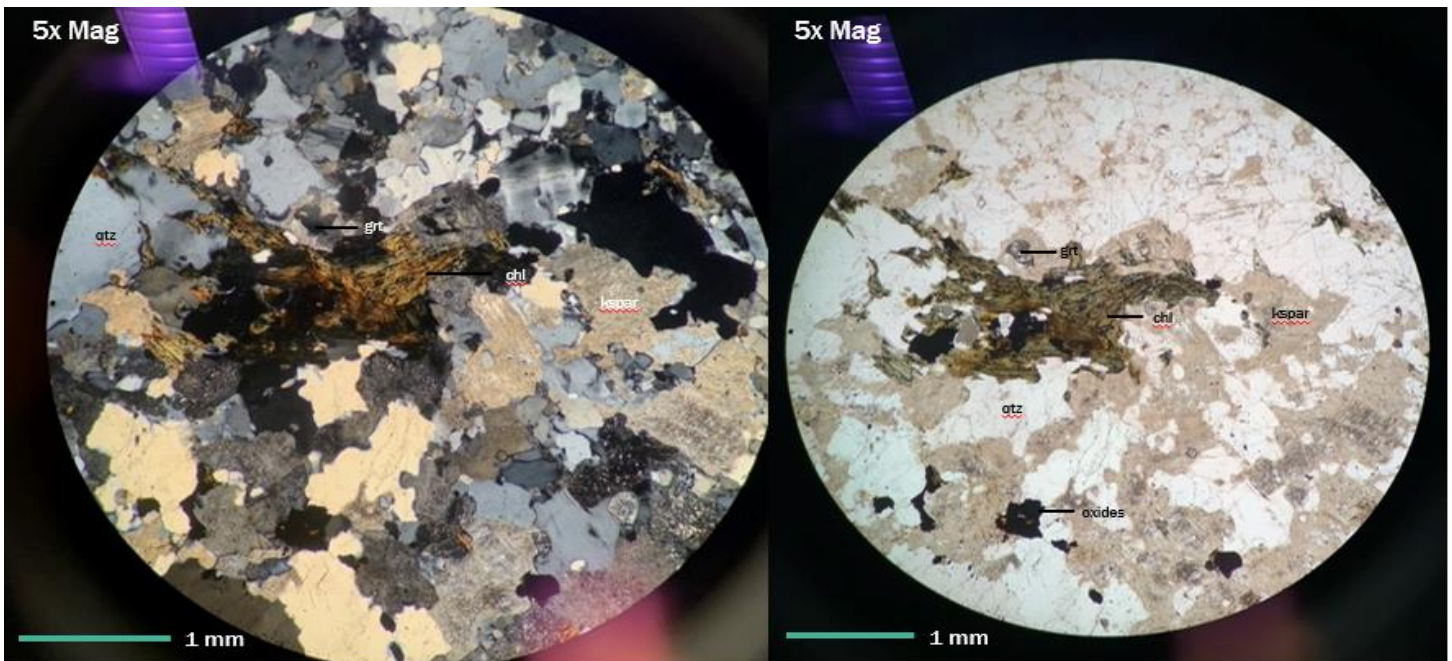


Figure 3. Sample Z2, showing mineral assemblage in plain-polarized and cross-polarized light. Source: Image taken by Julie Woods

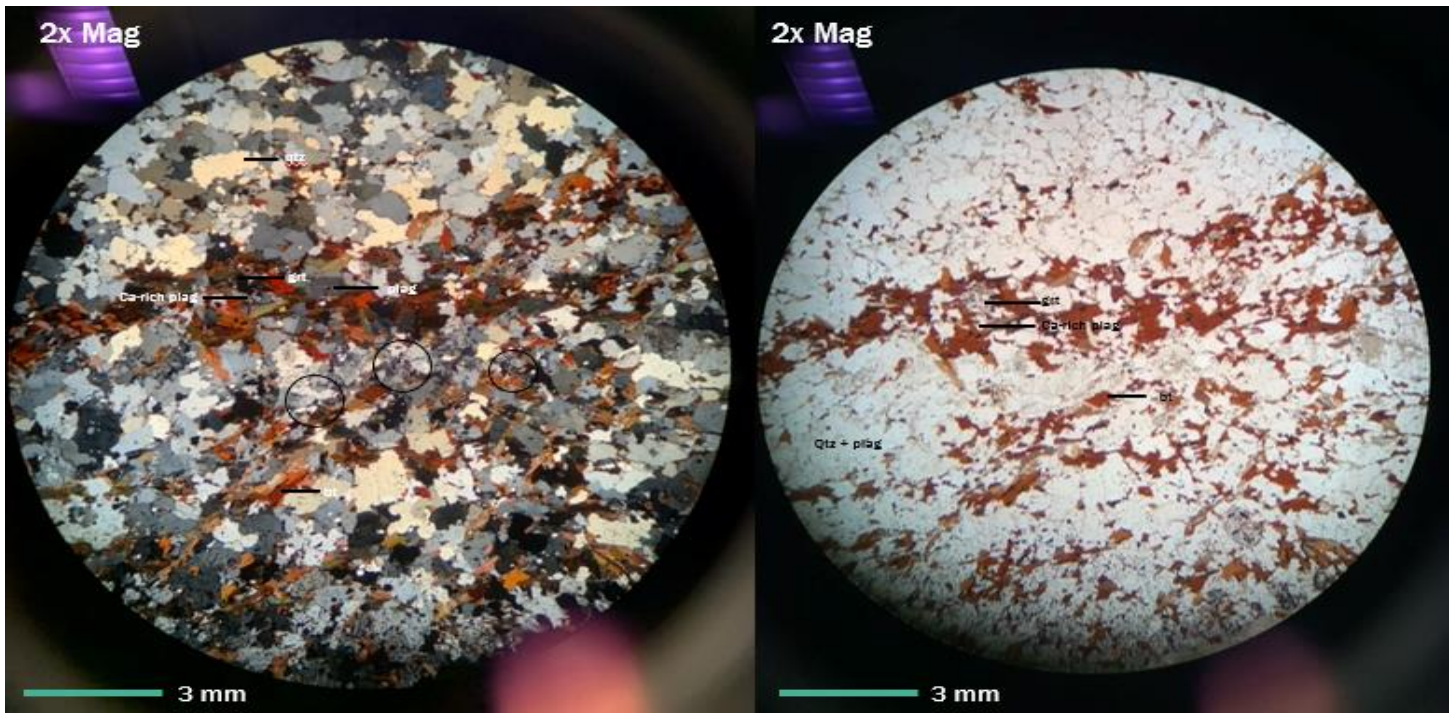


Figure 4. Sample Z14, showing mineral assemblage in plain-polarized and cross-polarized light. Circles denote areas of symplectite. Source: Image taken by Julie Woods

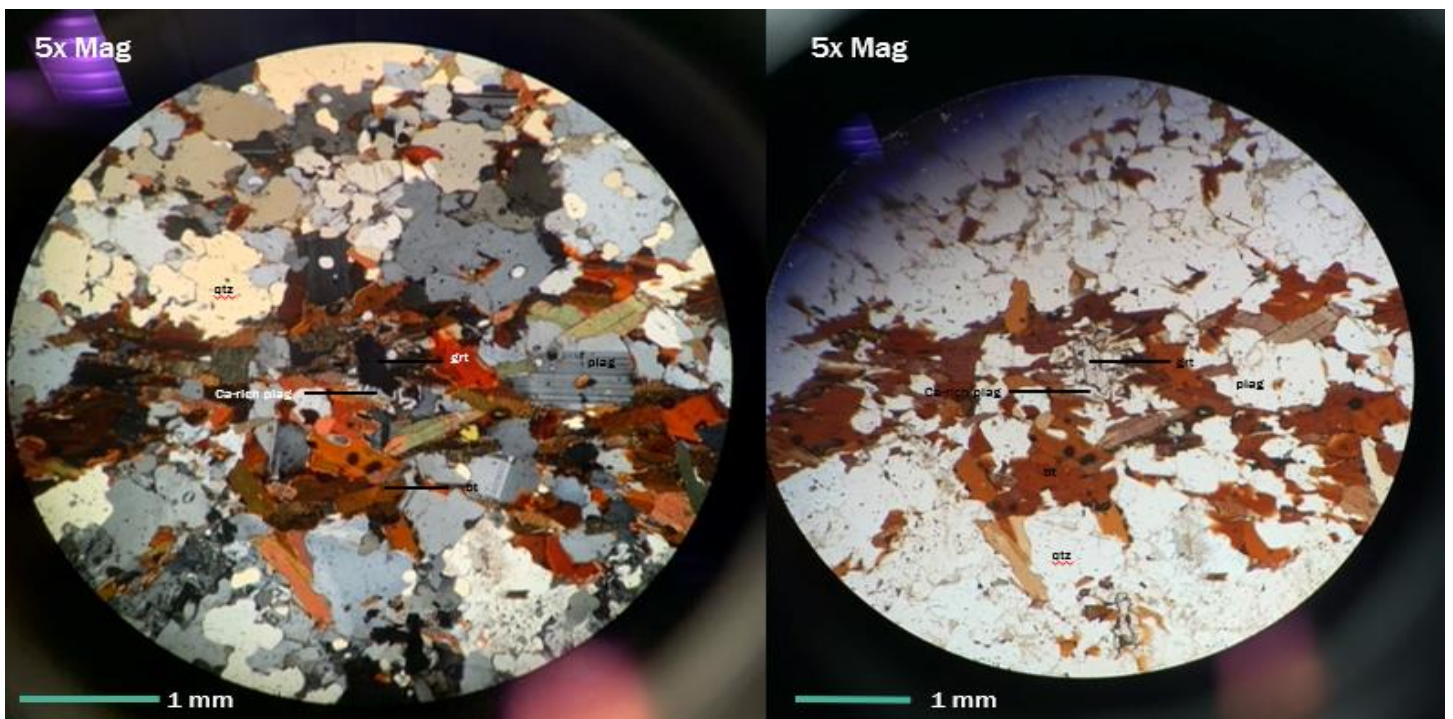


Figure 5. Sample Z14, showing garnet break-down present, and symplectic texture surrounding the grain. Source: Image taken by Julie Woods

5.2 X-Ray Mapping

For the purpose of this research, x-ray analysis was conducted on the garnet grains present in both Z2 and Z14. The x-ray analysis was carried out on the electron microprobe and was used to ascertain the Ca, Fe, Mg, Y, and Mn concentration and their distributions in and around the garnets. X-ray analysis of a selection of garnet grains from Z2 and Z14 have yielded the below results for the Ca, Fe, Mg, Y, and Mn concentrations:

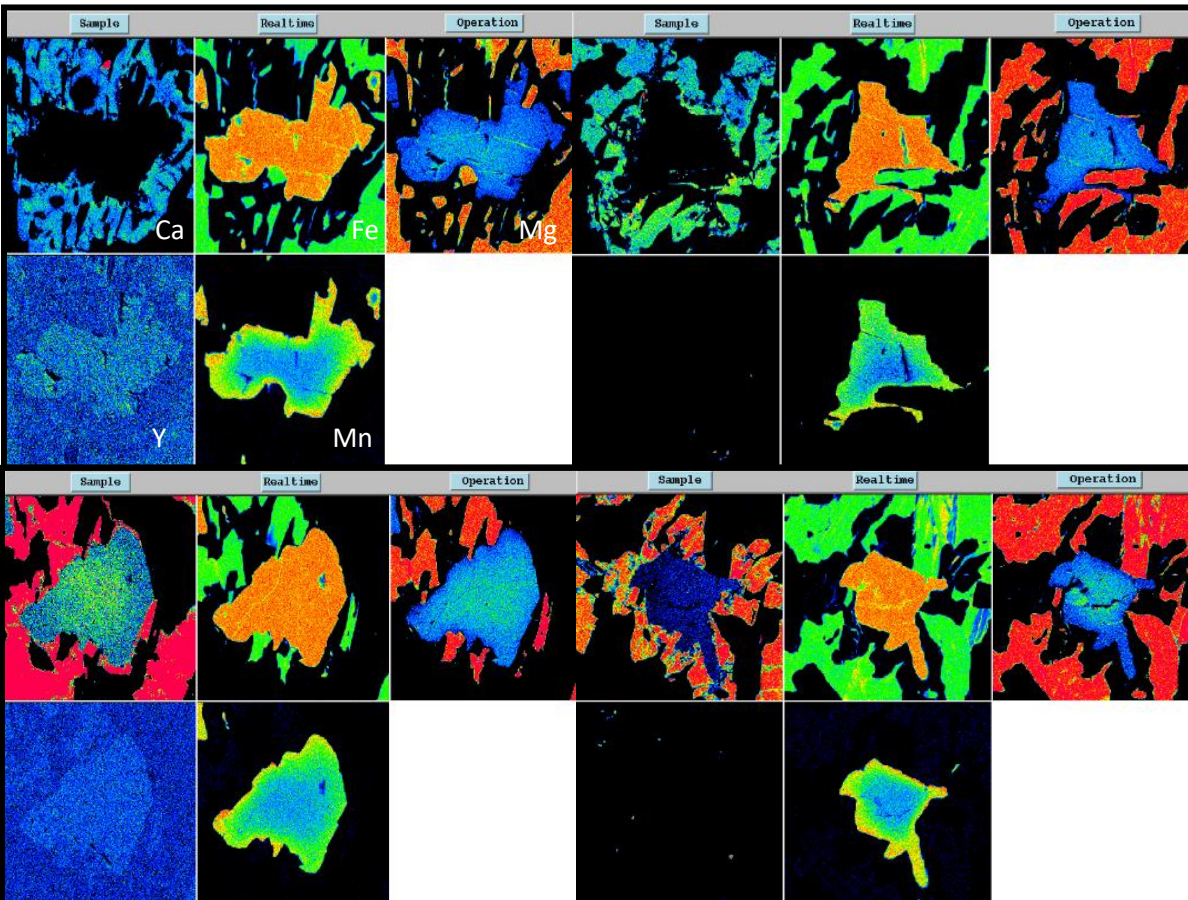


Figure 6. X-Ray maps of a selection of garnets from Z14, showing the concentrations of Ca, Fe, Mg, Y, and Mn. Source: Electron microprobe analysis conducted by Dr. Richard Cox

These maps show that overall, the garnet grains are showing high-Fe concentrations, with low-Ca and Mg, which are concentrating more in the surrounding plagioclase—with regards to the high-Ca—and the biotite—in terms of the high-Mg. Upon other analysis, it was determined that the Ca-rich end-member of plagioclase, anorthite, is only growing around the garnet grains where they are breaking down, as well as the Mg-rich biotite end-member, phlogopite. These x-ray maps are also showing an inversed Mn distribution from core to the rim: in

normal, prograde metamorphism, Mn-concentrations decrease from the core to the rim of the grain; the opposite is occurring in this instance in every garnet grain that has been analyzed for both Z2 and Z14.

5.3 Metamorphic Constraints

This section aims to explain the metamorphic constraints that were determined through this research, beginning with a brief description of the mineral classifications, which minerals were used for the classifications, and the plots and data tables as the supplementary information. Following this, the results of the geothermobarometric modelling will be discussed, as well as the error considerations for each model.

5.3.1 Mineral Classifications

In order to proceed with calculating temperatures and pressures of the samples, classification of the important mineral constituents have to be conducted first. The reason for conducting classification before the geothermobarometric modelling is to properly “match-up” pairs or groups of minerals that are in close proximity to one another that may have experienced the same metamorphic processes at time of deformation; this is to ensure that more accurate pressure and temperature conditions are calculated. The following sections explain and show the results of the classification of the garnet, biotite, plagioclase, and chlorite grains in sample Z2 and Z14:

Garnet classification

In order to classify the selection of garnet grains for the geothermobarometric models, the garnet end-members were plotted against one another in Triplot, which was done to examine the Fe, Ca+Mg, and Mn concentrations in the grains, using almandine, spessartine, and grossular and pyrope together. The grains that were used for this analysis were from both samples and the following plots show the relation between all four end-members:

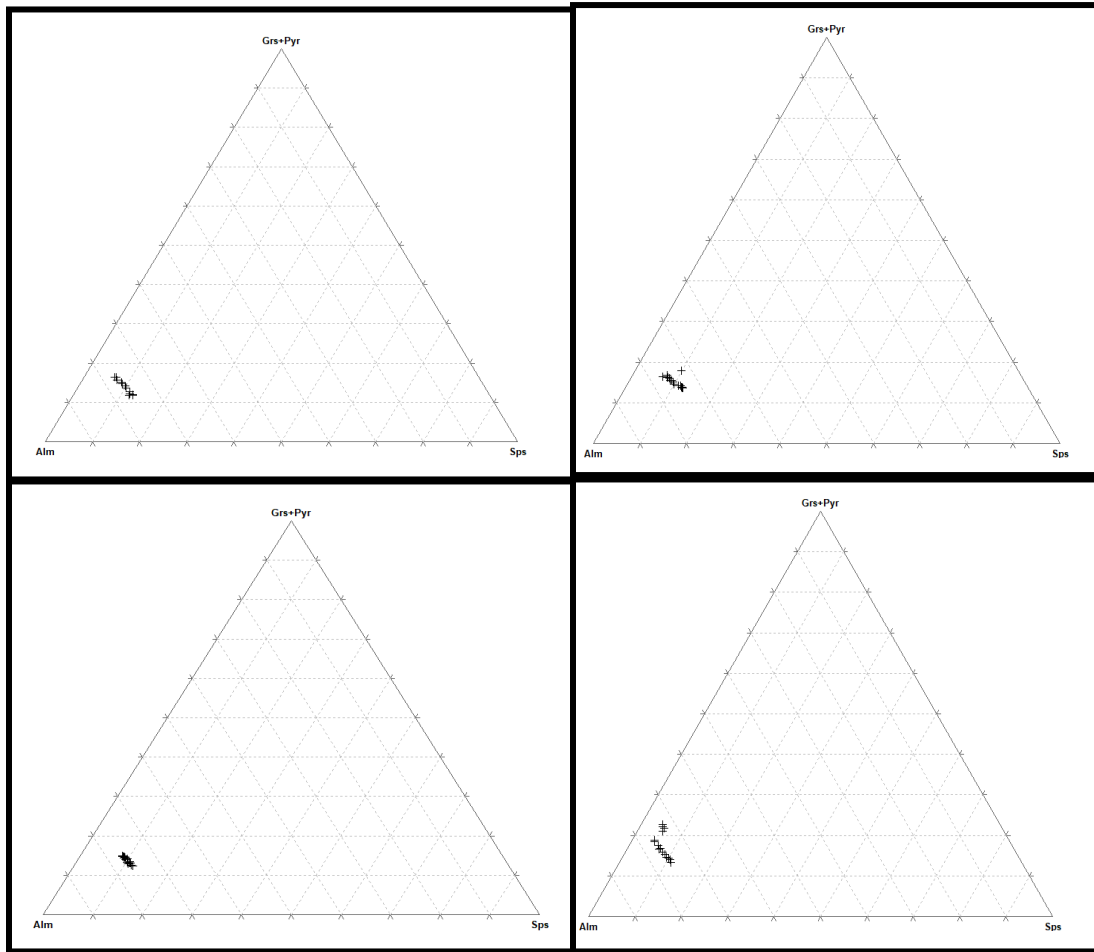
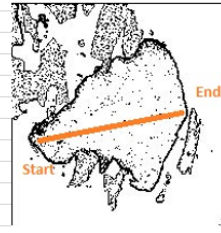


Figure 7. Garnet plots showing the concentrations of the different end-members: almandine, spessartine, and grossular and pyrope. Source: End-member concentrations were determined by Dr. Richard Cox and plots were created by Julie Woods

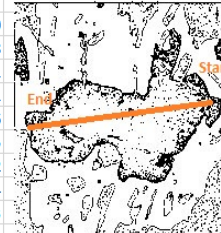
Overall, the plots are showing high concentrations of the Fe-rich end member, almandine, with much lower concentrations of the Mn-rich end-member, spessartine, and the Ca and Mg-rich end-members, grossular and pyrope respectively. The compositional average for the almandine end-member in each of the samples was plotted at approximately 77%, the compositional average for the spessartine end-member was approximately 7%, and the grossular and pyrope compositional averages together was approximately 16%. The following four data tables illustrates the individual element weight percentages for the selection of garnet grains that were classified, as well as the end-member distribution, and a line plot demonstrating the path the electron microprobe took during the analysis:

K2O	CaO	TiO2	Cr2O3	Na2O	MgO	Al2O3	FeO	MnO	SiO2	TOTAL	Grns	Prp	Alm	Sps	Gr+Prp
0.05	0.94	0.01	0.01	0.01	2.12	20.92	31.92	5.25	36.63	97.87	2.85	8.97	75.60	12.58	11.82
0.04	0.89	0.03	0.02	0.00	2.15	20.67	32.34	4.95	36.37	97.45	2.70	9.06	76.39	11.85	11.76
0.03	0.95	0.02	0.00	0.03	2.21	20.85	32.19	4.96	36.40	97.64	2.88	9.31	75.97	11.85	12.19
0.10	0.79	-0.01	-0.02	0.03	2.29	20.93	32.05	5.22	35.15	96.52	2.38	9.61	75.55	12.46	11.99
0.03	0.93	-0.01	0.01	0.00	2.26	20.87	32.66	4.99	36.63	98.38	2.77	9.40	76.07	11.77	12.16
0.03	0.96	0.00	0.00	0.00	2.38	20.87	32.44	4.90	36.51	98.07	2.88	9.88	75.67	11.57	12.76
0.03	0.95	-0.01	0.02	-0.01	2.65	20.91	32.90	4.37	36.59	98.41	2.80	10.93	76.04	10.23	13.73
0.03	0.97	-0.03	0.00	0.00	2.76	21.05	32.78	4.19	36.68	98.42	2.87	11.38	75.92	9.83	14.26
0.02	0.95	0.00	0.01	0.01	2.88	21.02	33.02	3.85	36.73	98.49	2.80	11.88	76.30	9.02	14.68
0.03	0.98	0.00	0.00	0.01	2.96	20.92	33.10	3.64	36.77	98.42	2.90	12.19	76.39	8.52	15.10
0.03	0.98	-0.01	0.01	0.01	3.08	20.96	33.07	3.43	36.83	98.37	2.89	12.67	76.41	8.03	15.56
0.02	1.03	-0.03	-0.02	0.02	3.26	20.92	33.37	3.11	36.76	98.44	3.02	13.31	76.45	7.22	16.33
0.04	1.00	-0.05	-0.01	0.00	3.26	20.98	33.30	2.96	36.93	98.41	2.95	13.39	76.74	6.92	16.34
0.02	1.06	0.00	-0.01	0.00	3.42	21.04	33.42	2.76	36.84	98.56	3.10	13.97	76.53	6.40	17.07
0.02	1.04	-0.04	0.01	0.00	3.42	21.15	33.65	2.67	36.84	98.76	3.03	13.93	76.86	6.18	16.96
0.02	1.04	0.00	0.00	0.00	3.51	20.95	33.62	2.58	36.95	98.69	3.04	14.28	76.72	5.96	17.32
0.03	1.07	-0.02	-0.01	0.00	3.56	21.11	33.73	2.51	36.88	98.86	3.12	14.41	76.67	5.79	17.54
0.02	1.06	-0.03	0.02	0.01	3.63	21.01	33.53	2.41	36.88	98.55	3.09	14.78	76.54	5.58	17.88
0.02	1.04	-0.02	-0.03	0.00	3.65	21.23	33.84	2.34	37.01	99.07	3.01	14.76	76.85	5.37	17.77
0.05	1.18	-0.02	-0.01	0.03	2.07	12.36	30.83	2.14	22.94	71.59	3.96	9.66	80.69	5.69	13.62
0.12	1.09	0.00	0.00	0.11	4.67	18.99	31.89	2.01	34.03	92.93	3.21	19.08	73.04	4.67	22.29



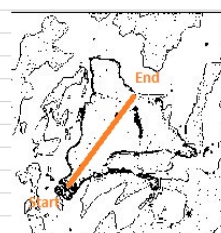
8 micron step size
70 points

K2O	CaO	TiO2	Cr2O3	Na2O	MgO	Al2O3	FeO	MnO	SiO2	TOTAL	Grns	Prp	Alm	Sps	Gr+Prp
0.04	1.12	0.01	-0.04	0.00	2.59	21.12	32.55	5.27	36.73	99.40	3.27	10.50	74.09	12.15	13.76
0.04	1.11	0.01	0.00	0.02	2.56	21.04	32.59	5.41	36.79	99.58	3.22	10.37	73.97	12.44	13.59
0.03	1.12	0.00	0.00	0.02	2.55	21.15	32.41	5.28	36.75	99.31	3.29	10.38	74.11	12.23	13.67
0.04	1.18	-0.03	-0.02	0.01	2.55	21.22	32.80	5.31	36.96	100.01	3.42	10.28	74.13	12.16	13.71
0.05	1.17	0.00	-0.03	0.02	2.60	21.06	32.77	5.16	36.88	99.66	3.39	10.50	74.27	11.84	13.89
0.04	1.21	-0.02	-0.01	0.01	2.66	21.11	33.00	5.09	36.77	99.85	3.49	10.67	74.25	11.59	14.15
0.04	1.18	0.00	0.00	0.00	2.68	21.05	32.91	4.80	36.65	99.32	3.43	10.85	74.70	11.03	14.28
0.66	1.42	0.05	-0.09	0.50	1.87	10.05	20.75	2.83	19.60	57.64	6.32	11.57	72.15	9.97	17.89
0.03	1.16	0.02	-0.01	0.00	2.80	21.23	33.56	4.38	37.18	100.33	3.35	11.21	75.46	9.98	14.56
0.02	1.22	-0.01	-0.02	0.00	2.90	21.26	33.35	4.13	37.00	99.85	3.52	11.67	75.34	9.46	15.19
0.02	1.28	-0.01	-0.03	0.01	2.96	21.12	33.68	3.97	36.93	99.93	3.67	11.83	75.49	9.01	15.50
0.03	1.24	0.00	-0.02	-0.01	2.95	21.18	33.66	3.81	37.21	100.06	3.58	11.86	75.86	8.70	15.44
0.04	1.25	-0.01	-0.02	0.01	3.08	21.17	33.45	3.64	37.15	99.75	3.62	12.40	75.64	8.34	16.02
0.04	1.27	0.02	-0.04	0.02	3.13	21.15	33.64	3.40	37.21	99.83	3.69	12.58	75.96	7.77	16.27
0.04	1.32	-0.01	-0.03	0.01	3.10	21.10	33.80	3.35	37.03	99.71	3.80	12.43	76.12	7.65	16.23
0.05	1.40	-0.02	-0.04	0.04	3.18	21.08	33.60	3.21	36.90	99.40	4.06	12.81	75.80	7.33	16.87
0.04	1.38	-0.01	-0.01	0.06	3.00	20.89	33.42	2.89	36.72	98.39	4.07	12.30	76.89	6.74	16.37
0.04	1.41	-0.02	-0.03	0.02	3.27	21.18	33.65	2.89	37.24	99.65	4.08	13.20	76.11	6.62	15.14
0.03	1.46	0.00	-0.05	0.00	3.33	21.07	33.87	2.86	37.14	99.70	4.19	13.30	76.01	6.50	15.22
0.03	1.46	-0.02	-0.02	0.02	3.35	21.25	33.94	2.74	37.10	99.86	4.19	13.41	76.16	6.24	15.32
0.03	1.40	0.00	0.01	0.02	3.30	21.13	33.89	2.63	37.09	99.50	4.06	13.30	76.61	6.03	15.41



6 micron step size
70 points

K2O	CaO	TiO2	Cr2O3	Na2O	MgO	Al2O3	FeO	MnO	SiO2	TOTAL	Grns	Prp	Alm	Sps	Gr+Pyr
0.03	0.92	-0.06	-0.02	0.02	2.35	21.01	33.17	5.18	36.30	98.91	2.71	9.58	75.74	11.97	12.29
0.04	0.90	-0.01	-0.02	0.03	2.47	20.96	33.40	4.93	36.53	99.21	2.61	10.01	76.02	11.36	12.62
0.03	0.91	0.00	0.03	0.01	2.57	21.11	33.38	4.82	36.59	99.44	2.64	10.40	75.87	11.09	13.04
0.02	0.91	-0.01	-0.01	0.01	2.54	20.90	33.30	4.70	36.41	98.78	2.66	10.35	76.10	10.89	13.02
0.04	0.92	-0.04	0.01	0.05	2.66	21.06	33.44	4.70	36.67	99.50	2.66	10.74	75.82	10.78	13.40
0.03	0.90	-0.01	0.00	0.03	2.63	20.93	33.53	4.49	36.54	99.05	2.62	10.66	76.36	10.36	13.28
0.04	0.91	-0.02	0.00	0.02	2.52	20.89	33.68	4.63	36.57	99.23	2.64	10.21	76.50	10.66	12.85
0.04	0.92	0.00	-0.02	0.03	2.84	21.08	33.52	4.28	36.71	99.39	2.67	11.49	76.02	9.83	14.15
0.03	0.88	0.00	0.00	0.03	2.83	21.04	33.54	4.17	36.49	99.01	2.56	11.49	76.33	9.61	14.06
0.03	0.95	-0.01	-0.04	0.02	2.93	21.04	33.78	4.06	36.62	99.37	2.73	11.78	76.21	9.27	14.51
0.03	0.90	0.00	0.02	0.02	2.93	21.01	33.93	3.98	36.66	99.47	2.59	11.77	76.56	9.09	14.36
0.03	0.90	-0.02	-0.01	0.03	2.97	20.98	33.50	3.88	36.76	99.01	2.62	12.08	76.34	8.96	14.70
0.03	0.94	-0.01	0.00	0.03	3.02	21.07	34.05	3.86	36.63	99.62	2.69	12.09	76.44	8.78	14.78
0.01	0.89	0.00	0.03	0.03	3.04	21.13	33.93	3.79	36.55	99.40	2.57	12.23	76.54	8.66	14.80
0.02	0.93	-0.02	-0.02	0.01	3.05	20.95	33.91	3.67	36.66	99.16	2.69	12.28	76.62	8.41	14.97
0.03	0.90	-0.02	0.00	0.02	3.05	21.00	34.11	3.73	36.71	99.53	2.60	12.22	76.67	8.50	14.82
0.03	0.89	-0.03	-0.01	0.01	3.09	21.02	34.05	3.80	36.86	99.72	2.57	12.35	76.45	8.63	14.92
0.02	0.87	-0.03	0.03	0.01	3.13	21.22	33.79	3.77	36.56	99.38	2.52	12.60	76.27	8.61	15.12
0.02	0.93	-0.03	-0.01	0.02	3.12	21.21	33.94	3.60	36.86	99.67	2.68	12.55	76.53	8.23	15.23
0.03	0.90	-0.01	0.00	0.03	2.99	21.25	33.92	3.62	36.92	99.66	2.61	12.11	76.96	8.32	14.72
0.02	0.91	-0.01	0.01	-0.01	3.18	21.19	33.80	3.52	36.77	99.37	2.63	12.81	76.50	8.07	15.44



6 micron step size
50 points

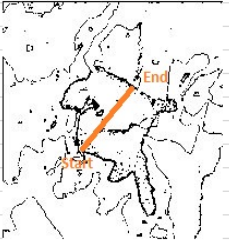
K2O	CaO	TiO2	Cr2O3	Na2O	MgO	Al2O3	FeO	MnO	SiO2	TOTAL		Grs	Prp	Alm	Sps	Gr+Pyr
0.04	0.96	0.01	-0.02	0.02	2.57	20.91	32.91	4.75	36.11	98.27		2.83	10.51	75.62	11.05	13.34
0.03	0.98	-0.02	-0.02	0.02	2.78	21.06	33.27	4.56	36.56	99.21		2.84	11.24	75.44	10.48	14.08
0.02	0.99	0.00	0.02	0.00	2.87	21.22	33.33	4.36	36.48	99.29		2.88	11.60	75.52	10.01	14.47
0.03	0.99	-0.03	-0.02	0.01	2.89	21.28	33.64	4.15	36.59	99.53		2.87	11.65	75.99	9.49	14.52
0.02	1.07	-0.02	0.01	0.03	3.08	21.16	33.85	3.84	36.58	99.61		3.07	12.30	75.92	8.71	15.37
0.03	1.08	-0.04	0.01	0.02	3.15	21.11	33.62	3.54	36.93	99.44		3.12	12.72	76.05	8.12	15.83
0.02	1.11	-0.03	-0.01	0.01	3.39	21.70	33.78	3.13	37.49	100.59		3.21	13.59	76.06	7.13	16.81
0.03	1.14	-0.05	-0.01	0.15	3.21	20.99	33.18	2.98	36.93	98.55		3.37	13.21	76.48	6.95	16.57
0.01	1.10	-0.02	0.00	0.03	3.61	22.18	34.08	2.75	38.02	101.75		3.14	14.40	76.23	6.23	17.54
0.02	0.82	-0.06	-0.07	0.24	4.13	21.80	28.15	2.08	36.96	94.09		2.73	19.04	72.77	5.46	21.77
0.04	1.08	-0.02	-0.02	0.19	4.02	22.08	29.94	2.16	38.25	97.71		3.40	17.63	73.59	5.38	21.03
0.11	1.07	-0.01	-0.01	0.18	4.42	21.07	30.64	2.07	36.79	96.34	7 micron step size	3.28	18.78	72.95	4.99	22.06
0.06	1.07	-0.04	-0.04	0.07	3.66	1.54	25.19	1.57	2.91	36.00	30 points	3.95	18.80	72.66	4.59	22.75
0.03	1.23	-0.04	-0.03	0.01	3.71	20.72	34.13	2.18	35.82	97.77		3.53	14.86	76.65	4.96	18.38
0.03	1.18	-0.04	-0.01	0.02	3.84	20.98	34.05	2.10	36.43	98.58		3.40	15.36	76.46	4.77	18.76
0.03	1.19	-0.03	0.02	0.02	3.75	21.06	33.91	2.16	36.65	98.76		3.43	15.09	76.54	4.94	18.52
0.06	1.20	-0.02	-0.01	0.07	3.78	20.50	33.51	2.12	36.02	97.22		3.49	15.33	76.30	4.88	18.82
0.02	1.20	-0.02	0.00	0.02	3.82	21.11	33.94	2.05	36.40	98.56		3.47	15.34	76.50	4.69	18.81
0.02	1.18	-0.02	-0.01	0.01	3.85	21.11	34.11	2.08	36.39	98.72		3.38	15.38	76.51	4.73	18.77
0.02	1.21	-0.05	0.00	0.01	3.83	21.24	33.87	2.14	36.53	98.80		3.49	15.38	76.25	4.89	18.87
0.01	1.20	-0.04	-0.01	0.00	3.77	21.35	34.07	2.13	36.43	98.92		3.45	15.12	76.58	4.86	18.57

Figure 8. Data tables and line plots of a selection of garnet grains from samples Z2 and Z14. Source: Data tables and line plots were produced from Dr. Richard Cox

The weight percentages for the corresponding element constituents for the garnet grains were then used in calculating the geothermobarometric models for the garnet-only, the garnet-biotite-plagioclase-quartz geobarometer, and the garnet-chlorite geothermometer.

Biotite Classification

Like the garnet classification, a selection of biotites were analyzed and classified based on their respective end-members: Mg-rich phlogopite, Fe-rich annite, Mg+Al-rich eastonite, and Fe+Al-rich siderophyllite. This was done to examine the different concentration and distributions of Fe, Mg, and Al in different biotite grains, located in the matrix and at close proximity to the garnet grains. The different values for the end-members were then plotted on a deer classification diagram, the following is said diagram:

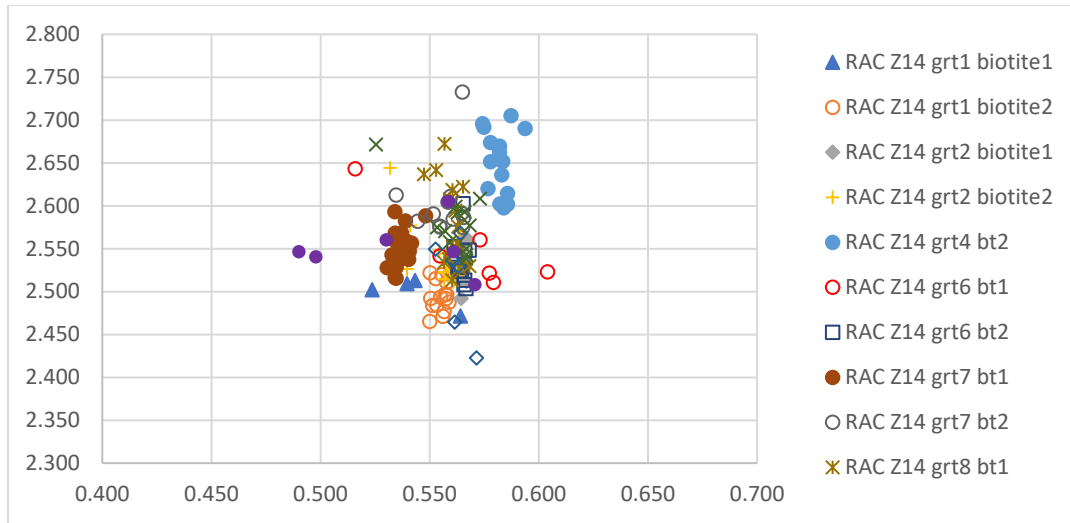


Figure 9. Graph of all biotites that were analyzed in samples Z14, using the Deer Classification (see Appendix). Source: Dr. Richard Cox

According to this classification, the biotite grains that were analyzed are showing high-Fe and Al concentrations, with no Mg being recorded (see supplementary data for an example diagram with labels). The following data tables illustrates the individual element weight percentages for the selection of biotite grains that were classified, as well as the end-member distributions:

T.Al	M.Al	M.Mg	M.Fe2+	M.Fe3+	Mn	Ti			Fe/Fe+Mg x2	Al IV x2		AlVI+Fe3++Ti	Mg	Fe2++Mn
1.256	0.429	1.017	1.211	0.099	0.160	0.011			0.543	2.513		0.539	1.017	1.371
1.255	0.473	1.014	1.188	0.025	0.172	0.009			0.540	2.509		0.507	1.014	1.361
1.251	0.504	1.043	1.146	0.000	0.171	0.007			0.524	2.502		0.511	1.043	1.317
1.236	0.469	0.964	1.247	0.063	0.150	0.014			0.564	2.472		0.546	0.964	1.397
1.246	0.470	0.988	1.211	0.036	0.166	0.010			0.550	2.492		0.516	0.988	1.377
1.261	0.457	1.001	1.224	0.060	0.163	0.011			0.550	2.522		0.529	1.001	1.387
1.242	0.472	0.991	1.218	0.037	0.172	0.009			0.551	2.484		0.518	0.991	1.390
1.258	0.481	0.984	1.217	0.038	0.164	0.010			0.553	2.515		0.528	0.984	1.380
1.260	0.482	0.984	1.230	0.027	0.164	0.008			0.556	2.520		0.517	0.984	1.394
1.244	0.483	0.980	1.241	0.018	0.159	0.009			0.559	2.488		0.511	0.980	1.400
1.238	0.484	0.974	1.223	0.030	0.161	0.009			0.557	2.477		0.523	0.974	1.384
1.242	0.476	0.980	1.214	0.038	0.163	0.009			0.553	2.484		0.523	0.980	1.378
1.248	0.485	0.976	1.231	0.031	0.166	0.009			0.558	2.496		0.525	0.976	1.396
1.247	0.488	0.974	1.215	0.040	0.162	0.009			0.555	2.494		0.537	0.974	1.377
1.236	0.489	0.976	1.222	0.027	0.160	0.008			0.556	2.471		0.524	0.976	1.382
1.255	0.479	0.979	1.235	0.032	0.161	0.010			0.558	2.511		0.521	0.979	1.396
1.249	0.488	0.969	1.220	0.032	0.159	0.009			0.557	2.497		0.529	0.969	1.378
1.246	0.475	0.974	1.227	0.046	0.157	0.009			0.558	2.492		0.530	0.974	1.385
1.233	0.466	0.992	1.213	0.042	0.159	0.009			0.550	2.465		0.517	0.992	1.372

Al IV	Mg	Fe 2+	Ti		X Fe	X Mg	X Al	X Ti		X ann	X phl	X eas	X sid
1.249525	1.00936	1.198036	0.009906	0	0.345571	0.291148	0.360423	0.002857	0	0.041268	0.02468	0.206226	0.290531
1.246924	0.981436	1.222647	0.009185	0	0.353347	0.283636	0.360363	0.002654	0	0.044117	0.022818	0.195689	0.3037
1.26621	0.94567	1.228808	0.009331	0	0.356174	0.274106	0.367015	0.002705	0	0.045184	0.020595	0.186133	0.314277
1.192058	0.911966	1.13553	0.006944	0	0.349771	0.280908	0.367183	0.002139	0	0.042791	0.022166	0.195575	0.303217
1.325456	0.908912	1.265762	0.009438	0	0.36066	0.258981	0.377669	0.002689	0	0.046913	0.01737	0.170983	0.331598
1.27502	0.952205	1.248859	0.009037	0	0.35834	0.27322	0.365847	0.002593	0	0.046014	0.020396	0.184344	0.317098
1.267649	0.960379	1.247396	0.007527	0	0.358143	0.275737	0.363958	0.002161	0	0.045938	0.020965	0.186787	0.315115
1.275413	1.033948	1.199407	0.004614	0	0.341382	0.294289	0.363016	0.001313	0	0.039785	0.025487	0.212215	0.285569
1.300898	0.974024	1.222508	0.007435	0	0.348803	0.277906	0.371169	0.002121	0	0.042437	0.021463	0.193496	0.304815
1.290618	0.960639	1.224023	0.00787	0	0.351413	0.275796	0.370532	0.002259	0	0.043396	0.020978	0.190242	0.308862
1.255916	0.952714	1.223327	0.009127	0	0.355506	0.276864	0.364977	0.002652	0	0.044931	0.021223	0.188844	0.311361
1.290643	0.96052	1.225383	0.007675	0	0.351695	0.275677	0.370425	0.002203	0	0.043501	0.020951	0.190023	0.309269
1.353753	1.121265	1.092562	0.008258	0	0.30554	0.313567	0.378583	0.002309	0	0.028524	0.030831	0.251262	0.238562

Figure 10. Data table used in the biotite classifications of a selection of grains from sample Z14. Source: Dr. Richard Cox

The weight percentages for the corresponding element constituents for the biotite grains, as well as the molar fractions of the end-members were then used in the garnet-biotite-plagioclase-quartz geobarometer to calculate pressure of the Z14 sample at time of deformation.

Plagioclase classification

Similar to the garnet classification, a selection of plagioclase grains was classified for the garnet-biotite-plagioclase-quartz geobarometer, which consisted of the plotting the end-members against one another in Triplot. This was done to examine the Ca, Na, and K concentrations in the grains, using albite, anorthite, and orthoclase. The grains that were used for this analysis were from sample Z14, either located in the matrix or to close proximity of the garnet grains, and the following plots show the relation between all three end-members:

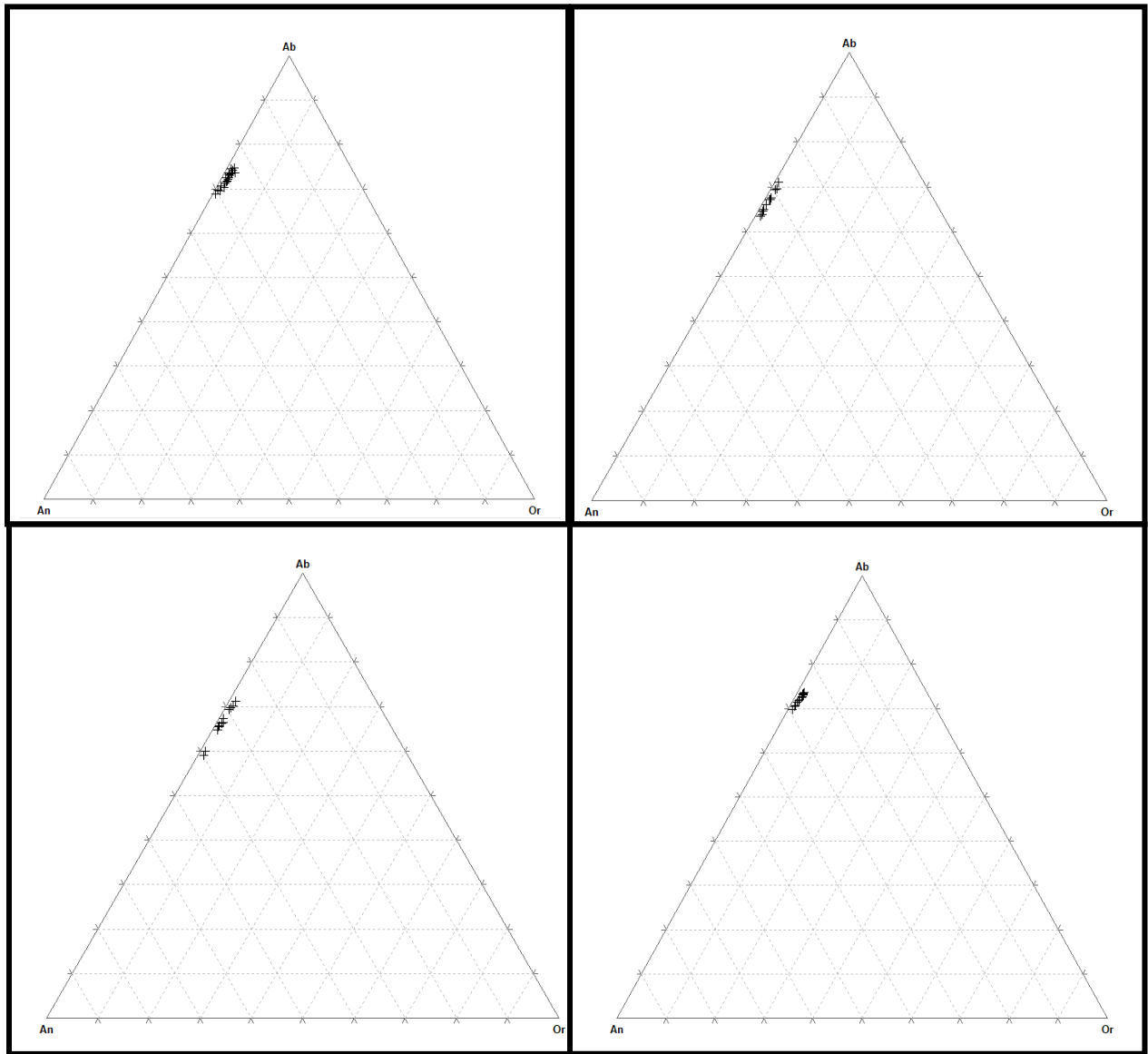


Figure 11. Plagioclase plots showing the concentrations of the different end-members: albite, anorthite, and orthoclase. Source: End-member concentrations were determined by Dr. Richard Cox and plots were created by Julie Woods

Overall, the plots are demonstrating high concentrations of the Na-rich end member, albite, with much some concentrations of the Ca-rich end-member, anorthite, and little to no and K-rich end-member, orthoclase. The compositional average for the albite end-member for each of the grains that were plotted was approximately 60%, the compositional average for the anorthite end-member was approximately 22%, and the orthoclase compositional average was approximately 2%. The following four data tables illustrates the individual element weight

percentages for the selection of plagioclase grains that were classified, as well as the end-member distribution:

K2O	CaO	TiO2	Cr2O3	Na2O	MgO	Al2O3	FeO	MnO	SiO2	P2O5	Cl	F	BaO	SrO	O	TOTAL
0.096343	6.36322	0.046869	0.009657	7.87137	-0.00974	24.7253	0.100815	0.016312	61.4574	0	0	0	0	0	0	100.678
0.100241	6.05999	0.024764	-0.01067	7.84541	-0.01289	24.8239	0.101846	0.012813	60.8237	0	0	0	0	0	0.000004	99.7691
0.113603	5.84644	-0.00535	-0.031	7.99288	-0.0112	24.4515	0.075962	0.000582	61.1216	0	0	0	0	0	0	99.5549
0.130059	5.45987	0.017403	-0.00102	8.16446	-0.01072	24.0081	0.067527	-0.00816	61.5032	0	0	0	0	0	0	99.3307
0.185476	5.30813	0.012715	0.018804	8.33871	-0.0083	24.0625	0.070165	-0.00757	61.3566	0	0	0	0	0	0	99.3372
0.155246	4.98023	0.026778	0.005084	8.39352	-0.00271	23.4399	0.057512	-0.00117	62.7154	0	0	0	0	0	0.000004	99.7697
0.254607	5.38122	0.018073	-0.01983	8.2745	-0.01608	24.3256	0.143662	-0.00466	61.5973	0	0	0	0	0	0.000004	99.9544
0.35117	4.76523	-0.01406	-0.01272	8.00589	0.005465	23.8045	0.070744	-0.00816	62.7001	0	0	0	0	0	0	99.6682
0.229082	4.5578	0.018751	-0.0173	7.88036	-0.01367	22.8443	0.079761	0.000583	61.4447	0	0	0	0	0	0	97.0244
0.247757	5.01062	-0.00268	-0.01882	8.39112	-0.0077	23.5952	0.069699	-0.01516	62.3478	0	0	0	0	0	0	99.6178
0.273904	5.06908	0.024782	-0.04476	8.30558	-0.00698	23.7019	0.076042	0.007579	61.8762	0	0	0	0	0	0	99.2833
0.149641	5.23404	-0.00134	-0.02443	8.33918	-0.00866	23.7711	0.063895	-0.0105	62.1418	0	0	0	0	0	0.000004	99.6548
0.225803	5.20219	0.007372	-0.02494	8.21061	-0.01417	23.912	0.050676	0.0035	61.9109	0	0	0	0	0	0	99.4839
0.257497	5.25111	0.01541	-0.04427	8.13412	-0.01153	23.7057	0.05542	-0.00233	61.814	0	0	0	0	0	0	99.175
0.269927	5.39722	0.02547	-0.02189	8.14801	0.002364	23.9673	0.044852	-0.00758	61.525	0	0	0	0	0	0.000008	99.3506
0.257252	5.38957	0.022805	-0.01375	8.02966	-0.00195	23.926	0.071372	-0.00525	61.8449	0	0	0	0	0	0	99.5207
0.260275	5.47607	0.015432	-0.00866	8.04029	-0.01298	24.1169	0.059736	0.015768	61.5509	0	0	0	0	0	0.000004	99.5138
0.233896	5.72538	0.02886	-0.00102	8.22986	-0.00844	24.158	0.062396	0.010513	61.1669	0	0	0	0	0	0.000004	99.6063
0.266523	5.59984	0.019458	-0.027	7.71008	-0.00938	23.9184	0.127007	-0.01401	60.2312	0	0	0	0	0	0	97.8221
0.203459	6.01329	0.014755	-0.01375	7.91889	-0.01659	24.1905	0.185717	-0.00875	60.5638	0	0	0	0	0	0	99.0513
0.243084	5.19952	0.020778	-0.02291	8.15945	-0.00527	24.0674	0.004971	-0.00408	62.8984	0	0	0	0	0	0	100.561

Figure 12 and 13. Data tables demonstrating the concentrations of different plagioclase grains and the end-members. Source: Dr. Richard Cox

MINERAL	END-MEM	END-MEM	END-MEM
Feldspar(Ab,An,C)	68.739	30.7074	0.553548
Feldspar(Ab,An,C)	69.6743	29.74	0.58571
Feldspar(Ab,An,C)	70.7435	28.5949	0.661541
Feldspar(Ab,An,C)	72.4624	26.7782	0.759463
Feldspar(Ab,An,C)	73.1849	25.7441	1.07101
Feldspar(Ab,An,C)	74.624	24.4679	0.908105
Feldspar(Ab,An,C)	72.4835	26.0491	1.46741
Feldspar(Ab,An,C)	73.6498	24.2247	2.1255
Feldspar(Ab,An,C)	74.6972	23.8741	1.42867
Feldspar(Ab,An,C)	74.1068	24.4536	1.43961
Feldspar(Ab,An,C)	73.5855	24.8179	1.59663
Feldspar(Ab,An,C)	73.6028	25.5283	0.86897
Feldspar(Ab,An,C)	73.0877	25.5899	1.32245
Feldspar(Ab,An,C)	72.5916	25.8964	1.51193
Feldspar(Ab,An,C)	72.0545	26.375	1.5705
Feldspar(Ab,An,C)	71.8396	26.6462	1.51429
Feldspar(Ab,An,C)	71.5479	26.9282	1.52384
Feldspar(Ab,An,C)	71.269	27.3984	1.33264
Feldspar(Ab,An,C)	70.2198	28.1831	1.59705
Feldspar(Ab,An,C)	69.6122	29.211	1.17674
Feldspar(Ab,An,C)	72.9001	25.671	1.42891

The weight percentages for the corresponding element constituents for the plagioclase grains were then used in calculating the geobarometric model for the garnet-biotite-plagioclase-quartz geobarometer.

Chlorite classification

For the purpose of this research a selection of chlorite grains was analyzed in order to input the values into a geothermometer, and unlike the three previous mineral classifications described in this section, there are no end-members of chlorite to classify, however, the main element constituents of chlorite that were

important to analyze for Mg and Fe, as the geothermometer being used examines the equilibrium exchange of Fe and Mg between chlorite and garnet. The follow data table shows the different weight percentages of each element constituents of the chlorite grains found in sample Z2:

	RAC Z2 ga	RAC Z2 ga	RAC Z2 ga	RAC Z2 ga	RAC Z2 ga	RAC Z2 ga	RAC Z2 ga	RAC Z2 ga	RAC Z2 ga	RAC Z2 ga	RAC Z2 ga	RAC Z2 ga	RAC Z2 ga	RAC Z2 ga	RAC Z2 ga
SiO2	25.6881	27.4622	27.1314	25.9834	26.7468	27.8887	24.6119	25.43	22.5019	27.3125	32.4364	28.6427	25.8747	24.9058	
TiO2	0.046042	0.462658	0.458809	0.421498	0.423116	0.060647	0.044464	0.5575	14.0002	0.636398	0.358491	0.099598	0.09254	0.043265	
Al2O3	18.4514	18.8435	18.8754	18.6969	18.5497	18.5727	18.6687	17.237	15.9661	19.0415	19.5774	18.9304	18.3451	18.1047	
Cr2O3	0.011061	0.053838	0.004182	-0.01611	0.018645	-0.00199	0.0251	0.0126	0.015305	0.00331	0.019089	0.030682	0.003243	0.010081	
Fe2O3	1.455141	1.952469	2.099924	2.212885	2.402922	3.556967	1.219037	2.3901	7.970405	2.535752	6.290169	3.719387	1.822298	1.150083	
FeO	29.321	26.46118	26.69509	26.35204	26.68334	23.98267	30.88655	23.197	17.42205	24.78651	19.54191	23.99952	28.19781	30.6665	
MnO	0.51706	0.565392	0.524522	0.534174	0.461128	0.361382	0.51822	0.4562	0.405873	0.472801	0.351554	0.396099	0.440318	0.476724	
MgO	8.78341	8.31868	8.59565	8.67892	8.39706	7.6454	7.50392	8.3406	6.87714	8.92118	7.33546	8.14492	8.82941	8.42832	
NiO	0	0	0	0	0	0	0	0	0	0	0	0	0	0	
ZnO	0	0	0	0	0	0	0	0	0	0	0	0	0	0	
CaO	0.125507	0.116503	0.11048	0.114193	0.102926	0.092425	0.088675	0.0761	0.144454	0.06443	0.080304	0.037462	0.036753	0.029043	
Na2O	0.04787	0.035993	0.014957	0.053326	0.019419	0.005668	0.006344	0.0143	0.02369	0.029458	0.017406	-0.0026	0.002661	-0.00676	
K2O	0.243533	1.87282	1.35853	0.584983	0.874823	1.20002	0.267217	1.1835	0.640422	1.42321	2.01806	1.21521	0.342563	0.081184	
BaO	0	0	0	0	0	0	0	0	0	0	0	0	0	0	
Rb2O	0	0	0	0	0	0	0	0	0	0	0	0	0	0	
F	0	0	0	0	0	0	0	0	0	0	0	0	0	0	
Cl	0	0	0	0	0	0	0	0	0	0	0	0	0	0	
H2O*	10.58492	10.86481	10.8357	10.56042	10.67933	10.62301	10.36277	10.027	10.79849	10.84437	11.45714	10.88778	10.543	10.40412	
Total	95.27504	97.01004	96.70464	94.17663	95.35921	93.9876	94.2029	88.922	96.76604	96.07142	99.48339	96.10116	94.5304	94.29306	
Si	5.785824	5.970158	5.927364	5.841892	5.936702	6.191591	5.666837	5.9973	4.865656	5.952046	6.609121	6.203857	5.843451	5.719204	
Al iv	2.214176	2.029842	2.072636	2.158108	2.063298	1.808409	2.333163	2.0027	3.134344	2.047954	1.390879	1.796143	2.156549	2.280796	
Al vi	2.714049	2.873451	2.852154	2.84727	2.847378	3.134425	2.759989	2.857	1.045732	2.916203	3.440012	3.11937	2.762764	2.638858	
Ti	0.007799	0.075643	0.075384	0.07127	0.07063	0.010126	0.007699	0.0989	2.276732	0.104301	0.054934	0.016224	0.015717	0.007472	
Cr	0.00197	0.009254	0.000722	-0.00286	0.003272	-0.00035	0.004569	0.0023	0.002617	0.00057	0.003075	0.005254	0.000579	0.00183	
Fe3+	0.246651	0.319432	0.345253	0.374421	0.401381	0.594289	0.21123	0.4242	1.29702	0.415868	0.964534	0.606266	0.309712	0.198751	
Fe2+	5.523157	4.810997	4.877488	4.955041	4.953236	4.452942	5.947582	4.5754	3.150627	4.517474	3.330071	4.347362	5.325801	5.88945	
Mn	0.098647	0.104114	0.097065	0.101731	0.086697	0.06796	0.10107	0.0911	0.07434	0.087276	0.060676	0.072671	0.084231	0.092728	
Mg	2.949075	2.695841	2.799352	2.908792	2.77837	2.530251	2.575569	2.9322	2.216764	2.898121	2.228065	2.629808	2.972454	2.885131	
Ni	0	0	0	0	0	0	0	0	0	0	0	0	0	0	
Zn	0	0	0	0	0	0	0	0	0	0	0	0	0	0	
Ca	0.03029	0.027138	0.025862	0.02751	0.024479	0.021987	0.021877	0.0192	0.033469	0.015045	0.017532	0.008694	0.008894	0.007146	
Na	0.041813	0.030344	0.012672	0.046495	0.016715	0.00488	0.005665	0.0131	0.019865	0.024895	0.013754	-0.00218	0.002331	-0.00602	
K	0.13993	1.038641	0.757143	0.335521	0.495351	0.679644	0.156956	0.712	0.353271	0.791212	1.048973	0.671457	0.197358	0.047558	
Ba	0	0	0	0	0	0	0	0	0	0	0	0	0	0	
Rb	0	0	0	0	0	0	0	0	0	0	0	0	0	0	
F	0	0	0	0	0	0	0	0	0	0	0	0	0	0	
Cl	0	0	0	0	0	0	0	0	0	0	0	0	0	0	
OH*	16	16	16	16	16	16	16	16	16	16	16	16	16	16	
Total	35.75338	35.98486	35.8431	35.66519	35.67751	35.49615	35.79221	35.726	34.47044	35.77096	35.16163	35.47492	35.67984	35.7629	

Figure 14. Data tables demonstrating concentrations for a selection of chlorite grains in sample Z2, used for the chlorite classification. Source: Dr. Richard Cox.

According to the major element analysis of the selection of chlorite grains from Z2, the grains are presenting with much more Fe concentrations than Mg. It is important to note that all data tables and plots present in this section are not completely representative of the whole data set used in the calculations of the geothermobarometric models, as the quantity of the data set was too large to insert into the paper. All data present in the tables were collected by Dr. Richard Cox, as well as the students from EARTH 2001 from previous analysis.

5.3.2 Garnet-Chlorite Geothermometer

As mentioned in previous sections of this paper, the garnet-chlorite geothermometer examines the fractionation of Mg and Fe in biotite and chlorite, which is then used to ascertain a potential geothermometer for garnet and chlorite (Ghent et al., 1987). The Mg and Fe concentrations in both the garnet and the chlorite grains that are being analyzed are then used in calculating the equilibrium constant which, with pressure conditions of the samples, can be inputted into the model for determining temperature conditions. The results of this analysis for sample Z2 produced temperature conditions that ranged from 550-600°C with an error of $\pm 25^\circ\text{C}$ as specified in the error consideration for the garnet-biotite geothermometer, which was explained as being proxy for the garnet-chlorite geothermometer. These conditions were then plotted to demonstrate the trend:

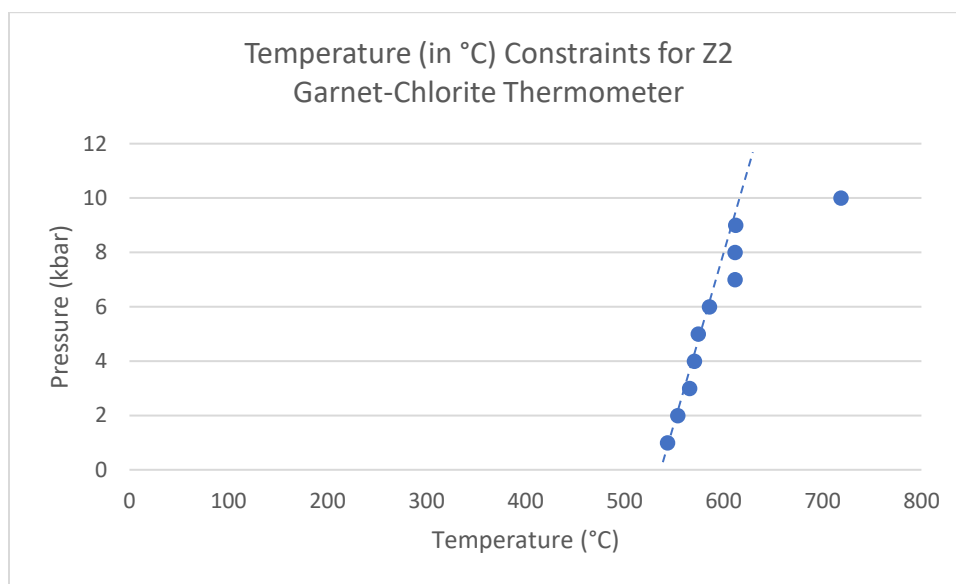


Figure 15. Graph created on Excel to plot the different temperatures recorded by the garnet-chlorite thermometer. Source: Data used for calculation was determined from Dr. Richard Cox, and calculation and plotting were conducted by Julie Woods

Overall, the trend of the temperature is showing a linear trend with one outlier plotting at around 740°C. The following data table shows the process of calculating the equilibrium constant and the final temperatures of the sample:

Sample Analysis#	Comments	Chlorite compositions		Garnet compositions		Calculated Kd		Grambling (1990)		Dickenson and Hewitt (1986)				Ghent et al. (1987)	
		Mg	Fe	Mg	Fe	(Mg/Fe) in grt	(Mg/Fe) in chl	Enter P (kbars)	Enter T (oC)	Zero	Enter P (kbars)	Enter T (oC)	Zero	gas constant	T (Calculated)
Z2	grt area 1	2.9491	5.5232	0.450	6.256	0.1348		2.312107	515	56.97	1	534	*****	19872	546.45
		2.6958	4.811	0.503	6.433	0.1394		3.147154	523	102.23	1	546	*****	19872	558.79
		2.7994	4.8775	0.540	6.502	0.1448		4.696495	532	183.50	1	560	*****	19872	574.46
		2.9088	4.955	0.589	6.519	0.1539		5.240937	547	206.14	1	582	*****	19872	595.95
		2.7784	4.9532	0.542	6.566	0.1471		6.914421	546	99.02	1	565	*****	19872	584.65
		2.5303	4.4529	0.619	6.564	0.1659		7.327467	575	122.65	1	612	*****	19872	627.26
	high Fe in Chl	2.5795	5.5271	0.529	6.529	0.2168		8.96991	640	201.42	1	737	*****	19872	740.60

Figure 16. Sample data table of chlorite concentrations used for the garnet-chlorite thermometer. Source: Dr. Richard Cox

Garnet-only Geobarometer

The garnet-only geobarometer utilizes Ca, Fe, Mg, Y, and Mn concentrations in the garnet grains from core to rim, and these values in conjunction with a set of estimated temperature conditions will yield pressure conditions for the samples. The calibration required for this model consists of an equilibrium exchange between the Fe-rich garnet end-member, almandine, the Mg-rich oxide titanite, with the Ca-rich garnet end-member grossular, ilmenite, which is Fe-rich, and quartz. This calibration assumes that quartz is forming in a pure phase and both oxides are very near pure phase; for that reason, they are omitted from the final calculation. The Fe and Ca equilibrium exchange between almandine and grossular, as well as the thermodynamic model used for this barometer will yield pressure conditions for the samples. The results of this analysis for sample Z2 and Z14 produced pressure conditions that ranged from 2.5-7.5 kbar with an estimated error of ± 0.1 kbar as specified in the error consideration for the garnet-only geobarometer. These conditions were then plotted to demonstrate the following trend:

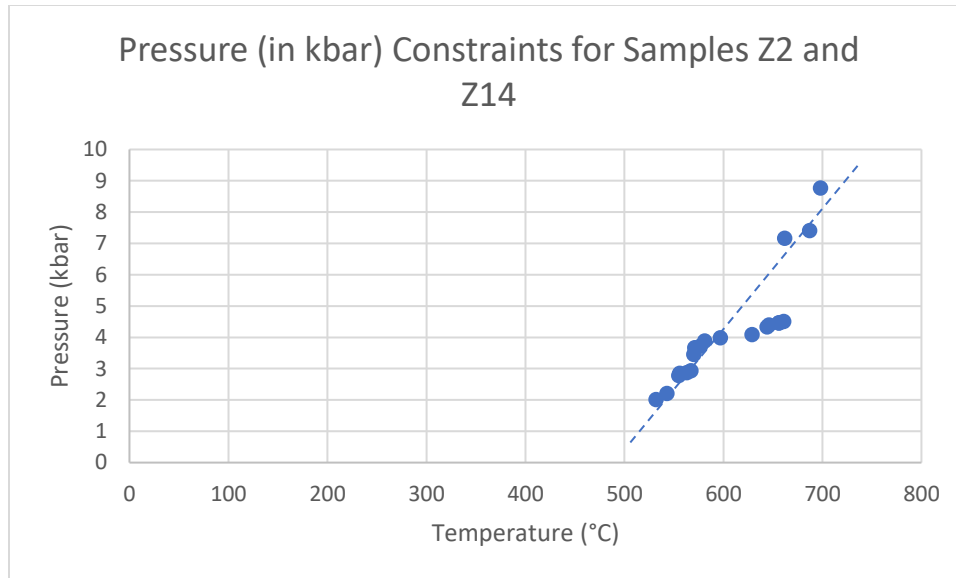


Figure 16. Graph created on Excel to plot the different temperatures recorded by the garnet-only barometer. Source: Data used for calculation was determined from Dr. Richard Cox, and calculation and plotting were conducted by Julie Woods

The following data table shows the data used for the garnet-only geobarometer:

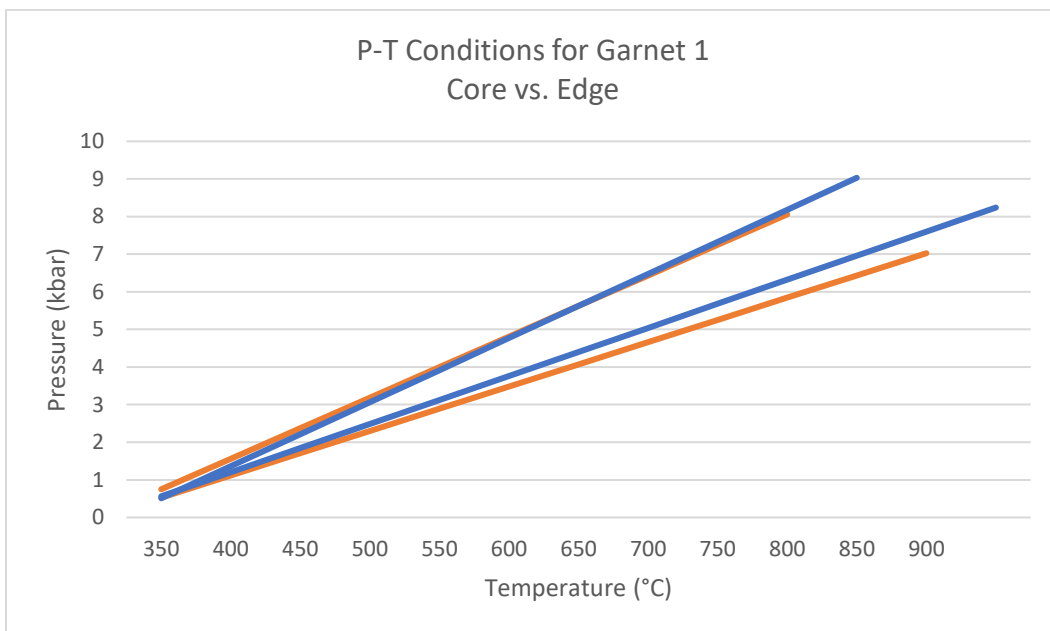
X Fe	X Mg	X Ca	X Mn	FeMg	FeCa	FeMn	MgCa	MgMn	CaMn	A	B	C	T	P (bar)	P (kbar)
0.671898	0.081983	0.032468	0.213651	0.055084	0.021815	0.143552	0.002662	0.017516	0.006937	-1.6288	-0.20248	3598.833	556	2312.107	2.312107
0.657651	0.081619	0.032433	0.228298	0.053676	0.02133	0.15014	0.002647	0.018633	0.007404	-1.70998	-0.2358	3714.61	570	2545.082	2.545082
0.665982	0.0795	0.039558	0.21496	0.052946	0.026345	0.143159	0.003145	0.017089	0.008503	-1.72074	-0.20457	3778.09	571	3147.154	3.147154
0.762073	0.128587	0.050802	0.058538	0.097993	0.038715	0.04461	0.006532	0.007527	0.002974	-1.29588	0.007698	3762.839	555	3436.215	3.436215
0.724026	0.180896	0.05855	0.036529	0.130973	0.042392	0.026448	0.010591	0.006608	0.002139	-1.68822	0.012635	5255.762	567	4392.83	4.39283
0.61715	0.346053	0.032083	0.004713	0.213567	0.0198	0.002909	0.011103	0.001631	0.000151	-3.16323	0.002846	10971.27	646	4696.495	4.696495
0.710278	0.238249	0.033255	0.018218	0.169223	0.023621	0.01294	0.007923	0.00434	0.000606	-1.73088	0.007679	6246.931	662	4033.263	4.033263
0.643293	0.320245	0.026051	0.01041	0.206011	0.016759	0.006697	0.008343	0.003334	0.000271	-2.67766	0.002337	9565.753	656	3814.464	3.814464
0.688558	0.273833	0.030124	0.007484	0.18855	0.020742	0.005153	0.008249	0.002049	0.000225	-2.04124	0.005192	7459.1	710	4534.431	4.534431
0.628496	0.331794	0.032134	0.007576	0.208531	0.020196	0.004762	0.010662	0.002514	0.000243	-2.94865	0.003271	10283.44	698	5240.937	5.240937
0.691601	0.257586	0.038884	0.011928	0.178147	0.026892	0.00825	0.010016	0.003073	0.000464	-2.01765	0.007782	7113.398	629	4319.239	4.319239
0.637928	0.315705	0.033795	0.012572	0.201397	0.021558	0.00802	0.010669	0.003969	0.000425	-2.76124	0.004071	9615.407	739	5836.511	5.836511
0.586608	0.383691	0.02708	0.002621	0.225076	0.015885	0.001538	0.01039	0.001006	7.1E-05	-3.74107	0.001327	12867.61	685	4978.154	4.978154
0.590054	0.37482	0.027681	0.007445	0.221164	0.016333	0.004393	0.010376	0.00279	0.000206	-3.62884	0.001797	12472.01	661	4691.799	4.691799
0.649947	0.312211	0.031975	0.005868	0.20292	0.020782	0.003814	0.009983	0.001832	0.000188	-2.61743	0.003734	9268.953	644	4301.308	4.301308
0.653613	0.312729	0.028947	0.004711	0.204403	0.01892	0.003079	0.009053	0.001473	0.000136	-2.56169	0.003025	9180.266	597	3346.856	3.346856
0.675962	0.280828	0.029742	0.013468	0.189829	0.020104	0.009104	0.008352	0.003782	0.000401	-2.17928	0.00467	7861.032	687	4306.603	4.306603
0.670583	0.148385	0.137201	0.043831	0.095905	0.092004	0.029392	0.020359	0.006504	0.006014	-2.52937	0.021212	6460.237	563	7327.467	7.327467
0.701928	0.139646	0.138927	0.019499	0.098021	0.097517	0.013687	0.019401	0.002723	0.002709	-2.384	0.029205	6016.738	543	6819.456	6.819456
0.696416	0.168812	0.113203	0.021569	0.117563	0.078836	0.015021	0.01911	0.003641	0.002442	-2.28747	0.023922	6204.533	581	6914.421	6.914421
0.679119	0.129895	0.071172	0.119815	0.088214	0.048334	0.081368	0.009245	0.015563	0.008527	-1.9583	-0.04449	5124.793	532	4562.022	4.562022

Figure 17. Data table of garnet concentrations and calculated variables used for the garnet-only barometer. Source: Initial concentrations were determined by Dr. Richard Cox, and calculations of variables were conducted by Julie Woods

5.3.3 Garnet-Biotite-Plagioclase-Quartz Geobarometer

The garnet-biotite-plagioclase-quartz geobarometer utilizes the Mg and Fe equilibrium exchange between garnet end-members and biotite end-member in order to calculate the pressure conditions, and these values in conjunction with a set of estimated temperature conditions will yield pressure conditions for the samples. The calibration required for this model consists of an equilibrium exchange between the Mg and Ca-rich garnet end-member,

pyrope and grossular, the Mg-Al-rich biotite end-member, eastonite, and quartz, with the Ca-rich plagioclase end-member anorthite, and the Mg-rich biotite end-member phlogopite as one part; the other consists of the equilibrium exchange between Fe and Ca-rich garnet end-members, almandine and grossular, the Fe-Al-rich biotite end-member, siderophyllite, and quartz, with the Ca-rich plagioclase end-member anorthite, and the Fe-rich biotite end-member, annite. This calibration assumes that quartz is forming in a pure phase and is omitted from the final calculation. The Fe and Mg equilibrium exchange between these constituents, as well as the thermodynamic model used for this barometer will yield pressure conditions for the samples. The results of this analysis for sample Z2 and Z14 produced pressure conditions that ranged from 1-9 kbar for the garnet cores (blue), and 1- 7 kbar for the rims (red). Two garnets were plotted to demonstrate the following trend:



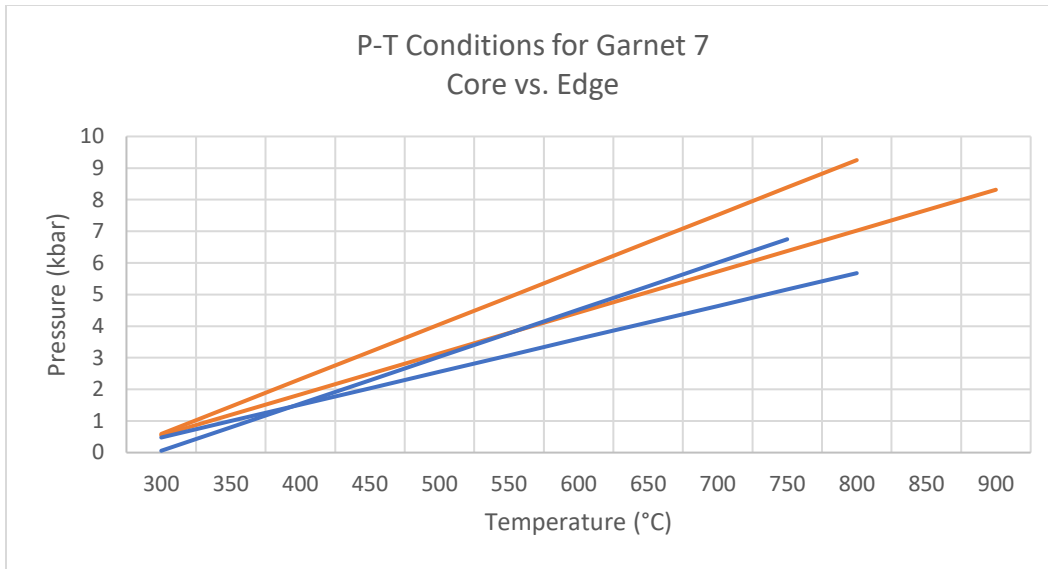


Figure 18. Two graphs showing the approximate PT conditions of two garnet grains from Z14, produced from the GBPQ barometer. Source: Initial concentrations used for calculations were determined from Dr. Richard Cox and calculations and plotting was conducted by Julie Woods

The following data tables for the two garnet grains are plotted below, presenting two sets of values for both cores and both rims:

T edge (Grt 1)	P edge (Grt 1)	T edge (Grt 1)	P edge (Grt 1)	T core (Grt 1)	P core (Grt 1)	T core (Grt 1)	P core (Grt 1)
350	0.527	450	0.749	300	0.563	400	0.509
400	1.117	500	1.561	350	1.203	450	1.361
450	1.708	550	2.373	400	1.843	500	2.213
500	2.299	600	3.185	450	2.482	550	3.065
550	2.889	650	3.997	500	3.122	600	3.917
600	3.48	700	4.809	550	3.762	650	4.77
650	4.071	750	5.621	600	4.401	700	5.622
700	4.661	800	6.433	650	5.041	750	6.474
750	5.252	850	7.245	700	5.681	800	7.326
800	5.843	900	8.057	750	6.32	850	8.178
850	6.433			800	6.96	900	9.03
900	7.024			850	7.6		

T core (Grt 7)	P core (Grt 7)	T core (Grt 7)	P core (Grt 7)	T edge (Grt 7)	P edge (Grt 7)	T edge (Grt 7)	P edge (Grt 7)
300	0.546	400	0.59	400	0.476	450	0.058
350	1.193	450	1.456	450	0.996	500	0.801
400	1.841	500	2.322	500	1.516	550	1.544
450	2.488	550	3.188	550	2.036	600	2.288
500	3.136	600	4.055	600	2.556	650	3.031
550	3.783	650	4.921	650	3.076	700	3.775
600	4.431	700	5.787	700	3.596	750	4.518
650	5.078	750	6.653	750	4.116	800	5.262
700	5.725	800	7.519	800	4.636	850	6.005
750	6.373	850	8.386	850	5.156	900	6.748
800	7.02	900	9.252	900	5.676		
850	7.668						
900	8.315						

Figure 19. Data tables for the two garnet grains that were used for the GBPQ barometer. Source: Dr. Richard Cox

Overall, the results of the barometers and the data tables ascertain that the garnet cores are yielding higher pressure conditions than that of the garnet rims.

Error considerations

The error considerations concerning the garnet-only geobarometer is in regard to the Fe³⁺ concentrations in the samples; if it is assumed that the Fe³⁺ accounts for 10-15% of the total iron found in the sample, it would introduce pressure errors ranging from ±0.05- 0.1 kbar. The fact of the matter is, Fe³⁺ concentrations in metapelites typically range from 0-5% of the total iron, which would result in the total error of the geobarometer to be equal to or less than ±1.3 kbar, which is generally the error determination for most geobarometers, such as the GASP model. Another source of error could come from the temperature calculations prior to running the geobarometric model, more specifically the garnet-biotite geothermometer, which is closely associated with this model. The total error associated with the garnet-biotite geothermometer is approximately ±25°C; this would result in pressure errors of approximately ±0.54 kbars (C.M Wu, 2019). The error considerations associated with the garnet-biotite-plagioclase-quartz geobarometer are similar to the GASP. These two barometers have a 1:1 ratio, meaning that both model present with error ranging of ±0.5-1.0 kbar (CM. Wu, et al., 2006).

6 Discussion

The textures that are present in the four thin sections are primarily describing a regional metamorphic history, with relation to the symplectic texture, the undulose extinction of the quartz and feldspars, and the schistosity of the micas. Despite this conclusion, the samples do present with some melting, but overall, it is not enough to classify the samples as having been affected by contact metamorphism from the Strontian granite intrusion. This is not to say that the Loch Eil and Glenfinnan groups were not affected by contact metamorphism, it is very likely that the samples collected were far enough away that they are outside of the contact aureole of the intrusion. If these samples had of been affected by Strontian granite intrusion, there would be granular and crystalline textures with no foliation, like what is associated with quartzites, as well as porphyroblasts, which are described as a

large mineral growth in a fine-grained matrix of a metamorphic rock (Streikeisen, 2006); these samples do not show such textures.

In terms of the geothermobarometry, before any of the modelling could proceed, classification of the main mineral constituents had to be conducted and then “matched-up” to one another depending on proximity and other conditions—which will be explained in this section—in order to ensure that more accurate pressure and temperature conditions were calculated. The reason for choosing grains that grew in close proximity to one another is due to the fact that that were likely affected by the same metamorphic event(s) and are exhibiting the same pressure-temperature conditions. The classification of garnets in the sample proceeded with x-ray mapping of a selection of grains and were produced from the electron microprobe. It was concluded with these maps that garnet resorption is being recorded when the Ca, Mg, and Mn concentrations were analyzed. According to these maps, low-Ca is being recorded in the garnet grains, but high-Ca is present in the surrounding plagioclase. It is assumed that the Ca is being absorbed from the garnets into the plagioclase due to the fact that upon major element analysis and plotting of the end-members: anorthite, albite, and orthoclase, the plagioclase located in the matrix is primarily Na-rich. The only location where there are higher concentrations of Ca in the plagioclase is around the broken-down garnet grains in Z14. As well in the x-ray maps, the biotite surrounding the garnet grains are consists of higher concentrations of Mg, while the garnet grains themselves have much lower concentrations. It is also assumed that this distribution is a result of garnet resorption due to the fact that upon classification of the biotite, and plotting of the end-members: annite, siderophyllite, phlogopite, and eastonite, the biotite located in the matrix of sample Z14 is primarily Fe and Fe+Al-rich with virtually no Mg present. Like the Ca-rich plagioclase, the only location where Mg-rich biotite is located in surrounding the broken-down garnet grains. Finally, the x-ray maps are presenting with inversed Mn distribution in the garnet grains from the core to the rim; in normal prograde metamorphism, Mn concentrations are higher in the core and then decrease towards the rim of the grain as temperature and pressure decreases, however Z14 is showing the opposite where the core of the garnet has lower concentrations of Mn, and increases towards the rim, which is likely indicative of a resorption texture of the

garnet due to multiple metamorphic events. The below diagram explains the normal prograde evolution (red curve) of the Mn concentrations from core to rim vs. the distribution that is occurring the garnet grains of Z14 (blue curve):

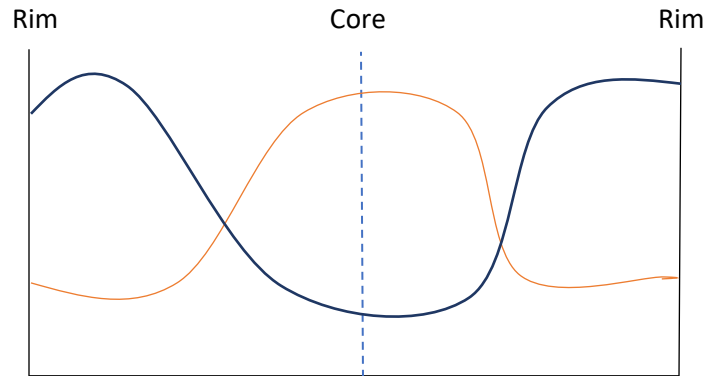


Figure 20. Graph showing the manganese (Mn) distribution from core to rim of a garnet grain: the red curve shows a normal distribution, and the blue curve shows the distribution in the garnet grains in sample Z14. Source: Information was interpreted from the x-ray maps produced by Dr. Richard Cox. Graph was produced from Julie Woods

Overall, the x-ray maps are showing multiple metamorphic events that are being recorded, however without any ages for the samples is it impossible to match the textures, and mineral assemblages to a specific metamorphic event and age of deformation.

Finally, in terms of the pressure-temperature conditions of the samples, they were determined through geothermobarometric modelling in the form of a garnet-chlorite geothermometer, a garnet-only and a garnet-biotite-plagioclase-quartz geobarometer. The results of these model produced temperatures ranging from 550-650°C with some outliers plotting around 750°C, and pressures ranging from 2-8 kbar, with some outliers plotting around 9 kbar, however most pressure that are being recorded in the samples are around 3-5 kbar. The results of the garnet-biotite-plagioclase-quartz barometer ascertain that the garnet cores are plotting much higher pressure than that of the rim. This in conjunction with the x-ray maps, it is appropriate to assume that the garnet grains were resorbed from other metamorphic events. It is also worth noting that the temperature and pressure conditions in the samples are the likely conditions of the most recent metamorphic event that deformed the samples, however, as it has been stated, it is impossible to verify without ages to corroborate. Overall, the pressure-temperature conditions of the samples appear to be of the

greenschist or amphibolite facies, but because it is assumed that these pressures and temperatures are indicative of the most recent event, this assessment may not be representative of the whole metamorphic history of this area. Any future analysis conducted on this topic will entail the use of other geothermometers and barometers; if any aluminosilicates are found within the samples, the GASP model could be utilized, as an example. As well, during this analysis, samples Z11 and Z13 were not used in any analysis aside the preliminary microscope and major element analysis; in the future, these samples could be used as a proxy for any missing information in Z2 and Z14, assuming they yield the same element concentrations within their mineral assemblages. Monazite analysis consisting of U-Th-Pb age dating will also be conducted in order to help ascertain, the ages of the mineral assemblages and the textures.

7 Supplementary Data

For calculating molar fractions and equilibrium constants for the GBPQ geobarometer:

C.M Wu, et al., 2006. "Empirical Garnet–Biotite–Plagioclase–Quartz (GBPQ) Geobarometry in Medium- to High-Grade Metapelites", page 1909 (table 1) and appendix formulas A1-12.

For calculating molar fractions and polynomials for the garnet-only geobarometer:

C.M Wu, 2019. "Original Calibration of a Garnet Geobarometer in Metapelite", page 3 formulas 5-7.

Example Deer Classification with labels:

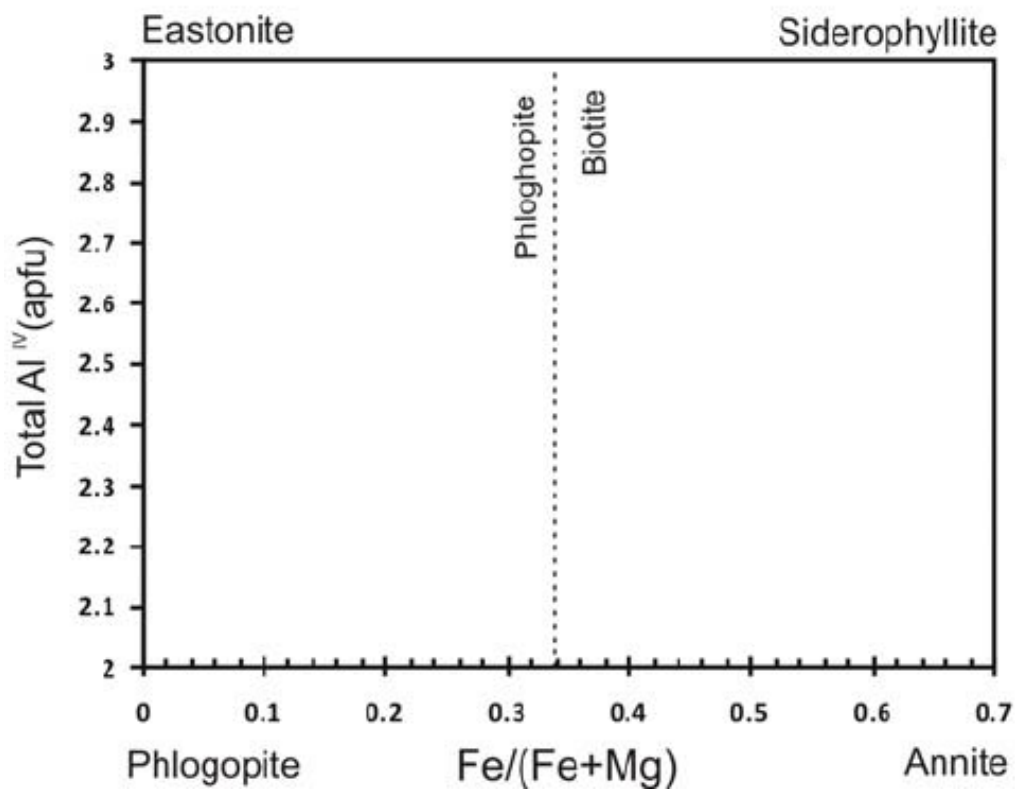


Figure 9. Deer Classification for biotites using end-members: eastonite, phlogopite, siderophyllite, and annite. This classification is used to plot the Mg, Al, and Fe concentrations in biotite grains. Source: M.H. Karimpour, et al., 2011

8 References

- Ashley, K. T., Law, R. D., & Thigpen, J. R. (2017). Garnet morphology distribution in the northern part of the Moine Supergroup, Scottish Caledonides. *Journal of Metamorphic Geology*, 35(1), 77–94. <https://doi.org/10.1111/jmg.12221>
- Ashley, K.T., Thigpen, J.R. & Law, R.D., 2015b. Prograde evolution of the Scottish Caledonides and tectonic implications. *Lithos*, 224–225, 160–178
- Bird, A.F., Thirlwall, M.F., Strachan, R.A. & Manning, C.J., 2013. Lu-Hf and Sm-Nd dating of metamorphic garnet: evidence for multiple accretion events during the Caledonian orogeny in Scotland. *Journal of the Geological Society*, 170, 301–317
- Bowes, D.R., 1968, The absolute time scale and the subdivision of Precambrian rocks in Scotland. *Geologiska Föreningens i Stockholm Förhandlingar*, v. 90, p. 175– 188, doi: 10.1080 /11035896809451881 .
- Brown, M. 2006. Duality of thermal regimes is the distinctive characteristic of plate tectonics since the Neoproterozoic. *Geology*, 34, 961–964.
- Brown, M. 2007. Metamorphic conditions in orogenic belts: A record of secular change. *International Geology Review*, 49, 193–234.
- Cawood, P. A., Nemchin, A. A., Strachan, R. A., Kinny, P. D., & Loewy, S. (2004). Laurentian provenance and an intracratonic tectonic setting for the Moine Supergroup, Scotland, 16 constrained by detrital zircons from the Loch Eil and Glen Urquhart successions. *Journal of the Geological Society*, 161(5), 861–874. <https://doi.org/10.1144/16-764903-117>
- Cawood, P. A., Strachan, R. A., Merle, R. E., Millar, I. L., Loewy, S. L., Dalziel, I. W. D., Kinny, P. D., Jourdan, F., Nemchin, A. A., & Connelly, J. N. (2014). Neoproterozoic to early Paleozoic extensional and compressional history of East Laurentian margin sequences: The Moine Supergroup, Scottish Caledonides. *Bulletin of the Geological Society of America*, 127(3–4), 349–371. <https://doi.org/10.1130/B31068.1>
- Cawood, P.A., Strachan, R.A., Merle, R.E. et al., 2015. Neoproterozoic to early Paleozoic extensional and compressional history of east Laurentian margin sequence: the Moine Supergroup, Scottish Caledonides. *Geological Society of America Bulletin*, 127, 349–371.

- Cutts, K. A., Kinny, P. D., Strachan, R. A., Hand, M., Kelsey, D. E., Emery, M., Friend, C. R. L., & Leslie, A. G. (2010). Three metamorphic events recorded in a single garnet: Integrated phase modelling, in situ LA-ICPMS and SIMS geochronology from the Moine Supergroup, NW Scotland. *Journal of Metamorphic Geology*, 28(3), 249–267. <https://doi.org/10.1111/j.1525-1314.2009.00863.x>
- Friend, C.R.L., Kinny, P.D., Rogers, G., Strachan, R.A. & Paterson, B.A., 1997. U-Pb zircon geochronological evidence for Neoproterozoic events in the Glenfinnan Group (Moine Supergroup): the formation of the Ardgour granite gneiss, north-west Scotland. *Contributions to Mineralogy and Petrology*, 128, 101–113.
- Friend, C.R.L., Strachan, R.A., Kinny, P.D. & Watt, G.R., 2003. Provenance of the Moine Supergroup of NW Scotland: evidence from geochronology of detrital and inherited zircons from sediments, granites and migmatites. *Journal of the Geological Society*, London, 160, 247–257.
- Ghent, E. D., & Stout, M. Z. (1987). *Chloritoid-bearing rocks associated with Blueschists and Eclogite, Northern Caledonia*. Retrieved March 26, 2022, from <https://onlinelibrary.wiley.com/doi/10.1111/j.1525-1314.1987.tb00382.x>
- Glendinning, N.R.W. 1988. Sedimentary structures and sequences within a late Proterozoic tidal shelf deposit: the Upper Morar Psammite Formation of northwestern Scotland. In: Winchester, J.A. (ed.) *Later Proterozoic Stratigraphy of Northern Atlantic Regions*. Blackie, Glasgow, 14–31.
- Sandiford, M., and Powell, R., 1986, Deep crustal metamorphism during continental extension: Modern and ancient examples: *Earth and Planetary Science Letters*, v. 79, p. 151–158
- Soper, N. J., Harris, A. L., & Strachan, R. A. (1998). Tectonostratigraphy of the moine supergroup: A synthesis. *Journal of the Geological Society*, 155(1), 13–24. <https://doi.org/10.1144/gsjgs.155.1.0013>
- Strekeisen, A. (n.d.). *Porphyroblastic Texture*. ALEX STREKEISEN-Porphyroblastic-. Retrieved March 25, 2022, from <https://www.alexstrekeisen.it/english/meta/porphyroblastic.php#:~:text=Porphyroblastic%20texture,local%20tectonic%20and%20metamorphic%20evolution.>
- Stoker, M. S. (1983). The stratigraphy and structure of the Moine rocks of eastern Ardgour. *Scottish Journal of Geology*, 19(3), 369–385. <https://doi.org/10.1144/sjg19030369>
- Strachan, R.A. 1986. Shallow marine sedimentation in the Proterozoic Moine succession, northern Scotland. *Precambrian Research*, 32, 17–33.

Strachan, R. A., Holdsworth, R. E., Krabbendam, M., Alsop, G. I., Road, B., & Po, P. (2010). The Moine Supergroup of NW Scotland: insights into the analysis of polyorogenic supracrustal sequences School of Earth and Environmental Sciences , University of Portsmouth , Reactivation Research Group , Department of Earth Sciences , The University , B. Group, 233–254.

Spear, F.S. (ed.) 1993. Metamorphic Phase Equilibria and Pressure–Temperature– Time Paths. Mineralogical Society of America, Monograph, 1

Vance, D. (1998). Extensional versus compressional settings for metamorphism: Garnet chronometry and pressure-temperature-time histories in the Moine Supergroup, northwest Scotland. *Geology*, 26(10), 927–930. [https://doi.org/10.1130/0091-7613\(1998\)0262.3.CO; 2](https://doi.org/10.1130/0091-7613(1998)0262.3.CO;2)

Wu, C.-M. (2019, September 6). *Original calibration of a garnet geobarometer in metapelite*. MDPI. Retrieved March 25, 2022, from <https://www.mdpi.com/2075-163X/9/9/540>

Wu, C.-M., Zhang, J., & Ren, L.-D. (2004, July 29). *Empirical garnet–biotite–plagioclase–Quartz (GBPQ) geobarometry in medium- to high-grade metapelites**. OUP Academic. Retrieved March 25, 2022, from <https://academic.oup.com/petrology/article/45/9/1907/1503588>

